UNIVERSIDADE
BEIRA INTERIOR

Development of co-delivery nanoparticles of temozolomide and plasmid DNA for glioblastoma treatment

VERSÃO FINAL APÓS DEFESA

Inês Sofia Patricio Afonso

Dissertação para obtenção do Grau de Mestre em
Ciências Biomédicas
(2º ciclo de estudos)

Orientador: Prof. Doutora Diana Rita Barata Costa
Coorientadoras: Prof. Doutora Ângela Maria Almeida De Sousa
Prof. Doutora Adriana Oliveira dos Santos

Março de 2025

Declaração de Integridade

Eu, Inês Sofia Patricio Afonso, que abaixo assino, estudante com o número de inscrição M12871 de Mestrado em Ciências Biomédicas da Faculdade da Beira Interior, declaro ter desenvolvido o presente trabalho e elaborado o presente texto em total consonância com o **Código de Integridades da Universidade da Beira Interior**.

Mais concretamente afirmo não ter incorrido em qualquer das variedades de Fraude Académica, e que aqui declaro conhecer, que em particular atendi à exigida referenciação de frases, extratos, imagens e outras formas de trabalho intelectual, e assumindo assim na íntegra as responsabilidades da autoria.

Universidade da Beira Interior, Covilhã 24 / 03 /2025

Inês Afonso

Dedication

Para ti mãe, que foste o meu porto de abrigo.

Acknowledgments

The completion of my master's degree marks the end of this journey, a process that has been filled with invaluable experiences and lessons. I could not have reached this point without the support and guidance of several people.

I want to express my deepest gratitude to my advisor, Professor Diana Costa, for her unwavering support throughout the past year and for imparting the scientific knowledge and experience I have gained. Her guidance was instrumental at every stage of my research. I would also like to thank my co-supervisors, Professors Adriana Santos and Angela Sousa, for their constant care, patience, and time spent in the lab and office answering my questions and clarifying doubts. Their presence and support made the entire process much more manageable.

I'm grateful to the University of Beira Interior, particularly the Health Science Research Center, for providing the facilities, equipment, and materials necessary for my research.

I would like to give special thanks to PhD student Ana Raquel, whose support throughout this year was exceptional. Ana's patience, compassion, and guidance taught me a great deal and helped me grow both professionally and personally. I also want to thank PhD student Tânia Alburquerque, whose support and mentorship were invaluable.
I'm also grateful to my fellow lab colleagues, whose camaraderie and contributions played a key role in my research journey.

I would also like to say a big thank you to my friends Beatriz Oliveira, Lucile Bonneau, Andressa Giusti and Diogo Pina who have given me emotional support throughout this year and who have become a second family. For all the nights studying in the library, all the hugs and words that motivated me to keep going.

Finally, I would like to thank my family, especially my mother, who showed how proud she was of me, who gave me strength and believed in me when I was not able to. Thank you for all the hours you spent on the phone with me saying "it's almost done, daughter, you can do it." I did it mom, thank you so much, I love you.

Resumo

A terapia génica é uma estratégia promissora e inovadora para o tratamento do cancro, particularmente para o glioblastoma, uma forma agressiva e altamente letal de cancro do cérebro com opções terapêuticas limitadas e um mau prognóstico. A combinação da terapia génica com a quimioterapia tem o potencial de amplificar os efeitos terapêuticos através da sua interação sinérgica, oferecendo uma abordagem mais eficaz para ultrapassar a resistência tumoral e melhorar os resultados dos doentes. Este estudo centrou-se no desenvolvimento de um sistema de co-entrega baseado em nanocomplexos TMZ-WRAP5/p53 revestidos com albumina bovina direcionado a células de glioblastoma. A temozolomida, um agente quimioterapêutico padrão para o glioblastoma, foi associada a um plasmídeo que codifica o gene supressor de tumores p53. O revestimento com BSA foi utilizado para aumentar a estabilidade, a biocompatibilidade e a eficiência de entrega dos complexos. Foi utilizada uma ferramenta de Desenho Experimental de forma a otimizar a formulação deste complexo, incluindo a relação N/P, a concentração e o tempo de adição de BSA. O processo de otimização envolveu a avaliação das principais propriedades, como o tamanho das partículas, a carga superficial e a capacidade de complexação do ADN. Determinou-se que a formulação ideal tinha um rácio (N/P) de 1,03 e uma concentração de BSA de 0,08%, resultando em complexos de aproximadamente 182 nm, um potencial zeta de +9,8 mV e uma eficiência de complexação de ADN de 96,5%. Estes complexos esféricos revestidos com BSA apresentaram uma elevada estabilidade e biocompatibilidade. Os estudos *in vitro* de biocompatibilidade e citotoxicidade com recurso a MTT, mostraram uma redução substancial da viabilidade das células do glioblastoma, sem toxicidade para os astrócitos. Os resultados de ensaios de PCR e qPCR mostraram um aumento significativo dos níveis de p53 em células de glioblastoma tratadas com o complexo revestido com BSA. Estes dados mostram que este sistema de entrega tem um potencial significativo para ultrapassar os desafios associados às terapias convencionais do glioblastoma.

Palavras-chave

Nanopartículas revestidas com BSA; péptidos WRAP; desenho experimental; terapia combinada; terapia do glioblastoma

Abstract

Gene therapy is a promising and innovative strategy for cancer treatment, particularly for glioblastoma, an aggressive and highly lethal form of brain cancer with limited therapeutic options and a poor prognosis. Combining gene therapy with chemotherapy has the potential to amplify therapeutic effects through their synergistic interaction, offering a more effective approach to overcoming tumor resistance and improving patient outcomes. This study focused on the development of a co-delivery system based on BSA-coated TMZ-WRAP5/p53 nanocomplexes targeting glioblastoma cells. Temozolomide, a standard chemotherapeutic agent for glioblastoma, was associated with a plasmid encoding the p53 tumor suppressor gene. BSA coating was used to increase the stability, biocompatibility and delivery efficiency of the complexes. An Experimental Design tool was used to optimize the formulation of this complex, including the N/P ratio, BSA concentration and addition time. The optimization process involved evaluating key properties such as particle size, surface charge and DNA complexation capacity. It was determined that the ideal formulation had an (N/P) ratio of 1.03 and a BSA concentration of 0.08%, resulting in complexes of approximately 182 nm, a zeta potential of +9.8 mV and a DNA complexation efficiency of 96.5%. These BSA-coated spherical complexes showed high stability and biocompatibility. *In vitro* biocompatibility and cytotoxicity studies using MTT showed a substantial reduction in the viability of glioblastoma cells, without toxicity to astrocytes. The results of PCR and qPCR assays showed a significant increase in p53 levels in glioblastoma cells treated with the BSA-coated complex. These data show that this delivery system has significant potential to overcome the challenges associated with conventional glioblastoma therapies.

Keywords

BSA-coated nanoparticles; WRAP peptides; design of experiments; combination therapy; glioblastoma therapy

Index

Figure List

Table List

List of Abbreviations

AAVs	Adeno-Associated Viruses
ADP	Adenosine Diphosphate
APNG	Alkylpurine-DNA-N-Glycosylase
ATP	Adenosine Triphosphate
AuNPs	Gold Nanoparticles
BAD	Bcl-2-Associated Death Promoter
BBB	Blood-Brain Barrier
BBD	Box-Behnken Design
BCL-2	B-cell lymphoma 2
BER	Base Excision Repair
CICS	Health Sciences Research Centre
CCD	Central Composite Design
cDNA	Complementary Deoxyribonucleic Acid
CNTs	Carbon Nanotubes
CTL	Cytotoxic T Lymphocyte
DLS	Dynamic Light Scattering
DISC	Death-Inducing Signaling Complex
DMEM- HG	Dulbecco's Modified Eagle Medium-High Glucose
DNA	Deoxyribonucleic Acid
ECM	Extracellular Matrix
ECs	Endothelial Cells
EDTA	Ethylenediaminetetraacetic Acid
EE	Encapsulation Efficiency
EGFR	Epidermal Growth Factor Receptor
EMT	Epithelial-to-Mesenchymal Transition
EPR	Enhanced Permeability and Retention
FBS	Fetal Bovine Serum
GBM	Glioblastoma Multiforme
Gp60	Glycoprotein 60
HIFs	Hypoxia-Inducible Factors
Mdm2	Mouse Double Minute 2
MGMT	O6-Methylguanine-DNA Methyltransferase
MSNs	Mesoporous Silica Nanoparticles
Mw	Molecular Weight

NK	Natural Killer
NSAID	Non-Steroidal Anti-Inflammatory Drug
NPs	Nanoparticles
O6-MeG	O6-Methylguanine
OXPHOS	Oxidative Phosphorylation
PBS	Phosphate Buffer Solution
P.I	Polydispersity Index
PIP3	Phosphatidylinositol (3,4,5)-Trisphosphate
PL3K	Phosphoinositide 3-Kinase
pDNA	Plasmid DNA
PTDs	Protein Transduction Domains
PTEN	Phosphatase and Tensin Homolog
QbD	Quality by Design
RAS	Rat Sarcoma Virus
RB	Retinoblastoma Protein
RNA	Ribonucleic Acid
RT-PCR	Reverse Transcription Polymerase Chain Reaction
RTK	Receptor Tyrosine Kinase
SDS	Sodium Dodecyl Sulfate
SEM	Scanning Electron Microscopy
SPARC	Secreted Protein Acidic and Rich in Cysteine
ST	Standard Deviation
TAE	Tris-acetate-EDTA
TB	Terrific Broth
TMZ	Temozolomide
TNFRSF	Tumor Necrosis Factor Receptor Superfamily
TNFSF	Tumor Necrosis Factor Superfamily
UBI	University of Beira Interior
VEGF	Vascular Endothelial Growth Factor
WHO	World Health Organization

List of Scientific Communications

Oral presentation

Inês Afonso, Ana R. Neves, Dalinda Eusébio, Tânia Albuquerque, Eric Vivès, Prisca Boisguérin, Adriana O. Santos, Ângela Sousa, Diana Costa. Optimization of bsa-coated peptide nanocomplexes using design of experiments for enhanced co-delivery of temozolomide and p53 gene. XIX Anual CICS-UBI Symposium. 16-17 July 2014, Covilhã, Portugal

List of Scientific Publications

Afonso, I., Neves, A. R., Eusébio, D., Albuquerque, T., Vivès, E., Boisguérin, P., Santos, A. O., Sousa, Â., & Costa, D. (2024). Design of Experiments to Tailor the Potential of BSA-Coated Peptide Nanocomplexes for Temozolomide/p53 Gene Co-Delivery. Pharmaceutics, 16(11), 1389. https://doi.org/10.3390/pharmaceutics16111389 (see chapter 7, figure 23)

Chapter 1- Introduction

1.1.1. What is Cancer?

Cancer is a complex group of diseases in which abnormal cells grow and spread out of control [1]. These cells can metastasize to other parts of the body, causing serious health complications [2]. Cancer is caused by an accumulation of genetic mutations that disrupt cell function, including cell cycle regulation, apoptosis, and DNA repair mechanisms mainly [3]. These mutations are either congenital or can be acquired due to environmental factors such as tobacco smoke, radiation, or for chemical and infectious reasons [3, 4].

Cancer is primarily a genetic disease, resulting from mutations in two major classes of genes: tumor suppressor genes (TSGs) and proto-oncogenes [5]. TSGs encode proteins that inhibit cell proliferation by mediating DNA repair, promoting cell cycle arrest, and inducing apoptosis [5]. Mutations or epigenetic silencing of TSGs result in loss of function, leading to unregulated cell growth and potential tumorigenesis [5]. Proto-oncogenes are normal genes that encode proteins that promote cell proliferation and growth [5]. When these genes undergo modifications, they turn into oncogenes, which can lead to the development of cancer cells [6]. The mutations that cause cancer can also appear in the genes responsible for DNA repair. When the DNA repair system fails, the damage persists for longer, which leads to genomic instability, genetic mutations and, eventually, carcinogenic transformation [7, 8].

The transformation of normal cells into cancer is not the only event important in the pathogenesis of cancer; instead, it is also the immune system failing to recognize and destroying newly created malignant cells while their numbers are still low [9]. Studies have shown that the risk of malignant neoplasms is significantly increased in individuals with suppressed immune systems due to factors such as chronic stress, advanced age, chronic frailty, prior medication use, and abuse of medications such as analgesics, antibiotics, and corticosteroids [10-13].

1.1.2. Hallmarks of cancer

The initiation and progression of tumors require metabolic reprogramming of cancer cells [14]. Cancer cells autonomously alter their flow through various metabolic pathways to meet the increasing bioenergetic and biosynthetic demand, as well as mitigate the oxidative stress necessary for cancer cell proliferation and survival [14]. The capabilities or "distinctive features" of cancer were first proposed by Hanahan and Weinberg in 2000. These authors analyzed the most acquired biological capabilities of cancer: uncontrolled proliferative signaling, resistance to apoptosis, initiating angiogenesis, acquiring replicative immortality, activating invasion and metastasis and evading growth suppressors (Figure 1). [15].

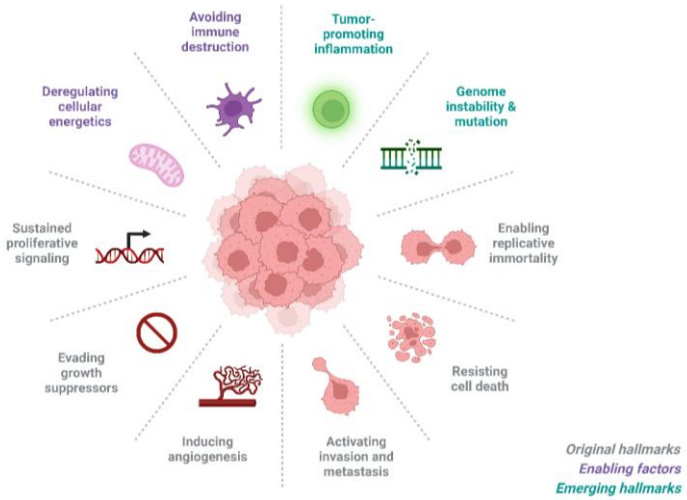

Figure 1 Original hallmarks of cancer, enabling factors and emerging hallmarks.

1.1.3. Warburg Effect

In 1927, Otto Warburg reported that cancer cells manifest a unique metabolic phenotype, characterized by a greater consumption of glucose compared to normal cells. This phenomenon became known as the "Warburg effect" [16, 17]. Cancer cells have a greater need for macromolecules to maintain their state of proliferation; thus, there is a greater need to synthesize or import macromolecules [18]. The metabolism of glucose allows for energy to be harnessed in the form of ATP through the oxidation of its carbon bonds in the mitochondria [19]. When oxygen is present, normal cells oxidize glucose to form ATP by means of glycolysis leading to the production of pyruvate [20]. The pyruvate is then taken through to the tricarboxylic acid cycle (TCA) and subsequently to oxidative phosphorylation (OXPHOS) where ATP is produced [21]. In the absence of oxygen, glucose is converted into lactate through anaerobic glycolysis. Cancer cells have the ability to enhance glycolysis to generate ATP with the production of lactate, regardless of the oxygen availability [22]. This allows the uncontrolled proliferation of cells, and the high production of lactate also leads to a decrease of pH generating an acidic microenvironment, where only cells with phenotypes resistant to acidic environments can grow [23]. Beyond metabolic reprogramming, cancer cells also exploit mechanisms such as angiogenesis to secure a continuous

supply of nutrients and oxygen, while evading apoptosis to sustain their uncontrolled growth and survival [24]. This intensifies the invasive and metastatic nature of cancer cells and offers a huge growth advantage as other cells around them deteriorate [23, 24].

1.1.4. Angiogenesis

Cancer can spread to adjacent or distant organs, which makes it life-threatening. Tumor cells can penetrate blood vessels and circulate through the intravascular current and then proliferate elsewhere: metastasis [25]. For the metastatic spread of cancerous tissue, the growth of the vascular network is important. The process of forming new blood vessels is called angiogenesis [26]. Angiogenesis is a process in which new blood vessels develop from existing capillaries, eventually creating a complete, regular and mature vascular network [27]. This process includes the degradation of the basement membrane and the activation, proliferation and migration of endothelial cells (ECs), which is regulated by various pro-angiogenic and anti-angiogenic factors [27]. One of the essential steps in tumor progression is the angiogenic switch, in which there is no longer a balance between pro-angiogenic and anti-angiogenic factors and there is an increase in pro-angiogenic stimuli, promoting tumor progression [28]. The increase in pro-angiogenic factors can occur due to low oxygen levels, as the rapid and uncontrolled proliferation of tumors limits oxygen availability, creating a hypoxic microenvironment [29]. Hypoxia has been shown to promote cell invasion and metastasis via epithelial–mesenchymal transition (EMT) [30]. Tumor cells in hypoxic conditions stabilize hypoxia-induced factors (HIFs), which in turn increase the expression of vascular endothelial growth factor (VEGF) and other pro-angiogenic genes [31, 32]. In addition, genetic mutations such as those in oncogenes and tumor suppressor genes can lead to increased production of angiogenic factors [33]. For example, mutations in the p53 tumor suppressor gene can result in reduced levels of thrombospondin-1, an anti-angiogenic factor, and with the increase of VEGF expression, thus tipping the scales in favor of angiogenesis [34].

1.1.5. Apoptosis

Apoptosis, or programmed cell death, is an essential mechanism for the maintenance of homeostasis, as it eliminates the damaged and potentially harmful cells [35, 36].
This mechanism is regulated by a network of specific genes and proteins and plays a crucial role in preventing diseases such as cancer by stopping the proliferation of abnormal cells [37]. Both extrinsic pathways (external stimuli through death receptors on the cell surface) and intrinsic pathways (mitochondria-mediated regulation after genotoxic stress) regulate the process of apoptosis through the regulation of various proteins, such as the members of the BCL-2 family. Dysregulation of these steps can result in the evasion of apoptosis [38].

The primary cells that induce the extrinsic pathway of apoptosis are natural killer (NK) cells and CD8 cytotoxic T lymphocytes (CTL) [39]. Both NK cells and CTLs are designed to eradicate infected or altered cells that are potentially tumorigenic [39]. The extrinsic apoptosis pathway is activated when tumor necrosis factor receptors (TNFRSF) bind to trimeric ligands of the tumor

necrosis factor superfamily (TNFSF) [39]. This leads to the formation of the membrane-bound death-inducing signaling complex (DISC) which activates caspases, cysteine-rich proteases that cleave intracellular proteins, initiating the cell death process [39]. Caspase-8, which is recruited and activated in the DISC complex, cleaves substrates such as caspase-3 [40]. Activated caspase-3 then cleaves actin, nuclear laminins and a DNase inhibitor, leading to DNA degradation, the interruption of cell division and migration and the cessation of nuclear functions, including the expression of survival genes [41].

The intrinsic pathway, also known as the mitochondrial pathway, is activated by internal stress signals, such as DNA damage or oxidative stress, which lead to the permeabilization of the mitochondrial membrane by pro-apoptotic proteins like Bax and Bak [42]. This allows cytochrome c to be released into the cytosol, where it binds with Apaf-1 to form the apoptosome, a complex that activates caspase-9 [43]. Caspase-9 then triggers a cascade of executioner caspases, like caspase-3, that break down cellular components, leading to the cell's orderly dismantling and eventual engulfment by phagocytes [44]. The intrinsic pathway is tightly regulated by the Bcl-2 family of proteins, which either promote or inhibit apoptosis, ensuring that cell death occurs only when necessary [44].

1.2. Glioblastoma

Despite advances, Glioblastoma remains the most lethal brain tumor accounting for 14.5% of all central nervous system tumors and 48.6% of malignant central nervous system tumors with a median survival of 14 months [45-48]. Gliomas are classified according to the glial cells that they morphologically most closely resemble, such as astrocytes (astrocytomas), oligodendrocytes (oligodendrogliomas) and ependymal cells (ependymomas). Considering this categorization, GBM is an astrocytoma [49]. Strong evidence suggested that glioblastoma arises from neural stem cells within the subventricular zone of the brain [50]. Defining histopathologic features are necrosis and endothelial proliferation, resulting in the assignment of grade IV, the highest grade in the World Health Organization classification of brain tumors [51]. For this, can strongly contribute factors such as the intra- and intertumoral heterogeneity, the presence of glioma stem cells relevant in tumor progression and treatment resistance, DNA damage repair mechanisms and the blood-brain barrier – a biochemical and biophysical barrier which limits drug penetration and, thus, drug efficacy [52-55]. GBM can be divided into primary and secondary types based on clinical characteristics [56]. Primary GBMs arise *de novo*, without any clinical or histological evidence of a precursor lesion [57]. In contrast, secondary GBMs develop gradually from pre-existing low-grade astrocytomas, progressing over time to a more aggressive form [57]. Typical molecular changes in glioblastoma include mutations in genes regulating receptor tyrosine kinase (RTK)/rat sarcoma (RAS)/phosphoinositide 3-kinase (PI3K), p53, and retinoblastoma protein (RB) signaling [51]. GBM is an extremely angiogenic and permeative tumor. Blood arteries are invaded by cells to promote the growth of tumors (co-option). Pericyte stability is

changed and astrocyte endfeet is displaced by GBM, resulting in perivascular niches and cell evasion [58] (Figure 2).

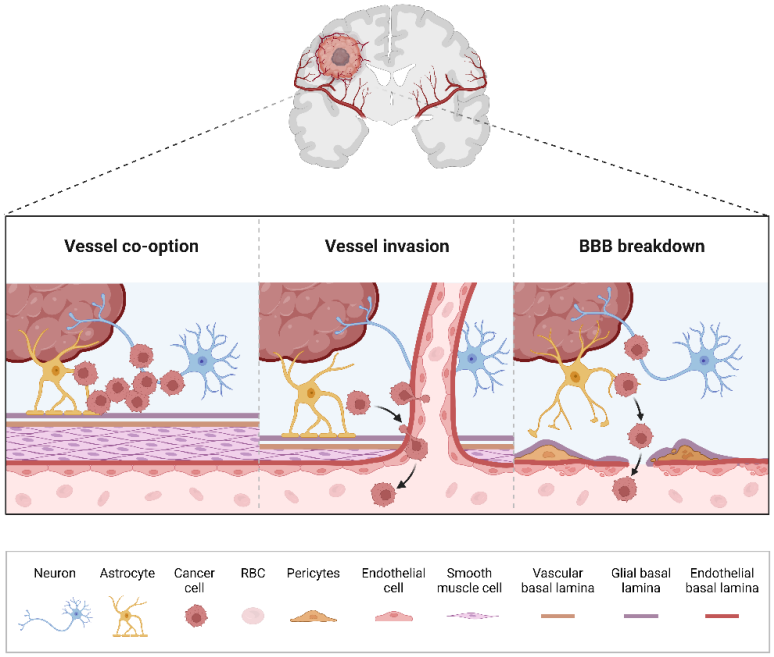

Figure 2. Graphical representation of Glioblastoma (adapted from [58]).

1.2.1 Risks and preventive measures

The risk factors of GBM include body mass index, alcohol consumption, exposure to magnetic fields and use of nonsteroidal anti-inflammatory drug (NSAID) [59]. A cohort study of 1.8 million Norwegians concluded that one risk factor of GBM is height, with a 24% increase in risk for every 10 cm in height. However, this association was not observed with BMI or gliomas with IDH mutations [60]. Other study explored the relationship between alcohol consumption and the risk of glioblastoma, using data from 39,766 participants in the Melbourne Collaborative Cohort Study over an average of 15 years [61]. The results indicated a significant dose-response relationship, in which higher alcohol consumption was associated with a higher risk of glioblastoma, specifically, every additional 10 grams of alcohol per day increased the risk by 16%, with people who consume 40-59 grams per day having a risk three times higher than people who abstain for life [61]. The results suggest that higher alcohol consumption can significantly increase the risk of this aggressive brain cancer [62]. Besides that, other population-based case-control study investigated the relationship between occupational exposure to magnetic fields and brain cancer in men with an incidence of different histological types [63]. Data was collected on 543 cases and 543 controls, matched by age and categorized based on average exposure to magnetic fields [63]. A significantly elevated risk was observed for glioblastoma multiforme, with a cumulative exposure index also significantly linked to this type of brain cancer [63, 64]. The use of NSAIDs suggests controversial results [65, 66]. A study gathered data to explore the relationship between factors related to the immune system, the use of medication and the risk of glioma [66]. Prolonged use of

antihistamines was found to be associated with a significantly increased risk of anaplastic gliomas, particularly among people with no history of asthma or allergies [66]. On the other hand, the use of anti-inflammatory drugs was associated with a reduced risk of glioblastoma, especially in people without asthma or allergies [66, 67]. These results suggest that common medications, such as antihistamines and anti-inflammatory drugs, can influence the risk of specific subtypes of brain tumors by modulating the immune system [66].

The causes of glioblastoma continue to be studied to this day with controversial results, so there is no specific way to prevent this disease, however, there are daily actions that can help prevent and/or reduce the likelihood of developing cancer [68]. One way is to maintain a healthy diet rich in nutrients to maintain a balanced weight, since excess weight is a predominant factor in the development of cancer [69-71]. Some studies even suggest that the Mediterranean diet can be beneficial for brain health [72]. Regular physical activity also improves general well-being and can reduce the risk of various types of cancer [73]. Alcohol consumption is one of the most important preventable risk factors for cancer, along with tobacco consumption [68]. Tobacco smoke contains a mixture of chemical substances, including reactive oxygen and nitrogen species (ROS and RNS), among others, which can cause cell damage [74]. Once in the body, alcohol can be converted into acetaldehyde, a chemical that can damage the DNA inside cells, which can lead to the development of cancer [75]. Alcohol consumption can also cause oxidative stress in cells, leading them to create more ROS [76].

1.2.2. Conventional Therapies: Temozolomide

The first-line therapeutic approach includes surgery, followed by radiotherapy and/or chemotherapy, almost in all situations using temozolomide an alkylating drug which delivers a methyl group to purine bases of DNA (O6-guanine; N7-guanine and N3-adenine) [76-78]. The main advantages are its lipophilic properties and small size that confer the ability to cross the blood-brain barrier [79]. Furthermore, this agent has demonstrated activity not only in brain tumors but also in a variety of solid tumors [79].

After being absorbed by the body, TMZ is degraded to form monomethyl triazene 5-(3-methyltriazen-1-yl)-imidazole-4-carboxamide (MTIC), MTIC reacts with water to release 5-aminoimidazole-4-carboxamide (AIC) and the highly reactive methyldiazonium cation [80] (Figure 3). The methyldiazonium cation preferentially methylates DNA at the N7 positions of guanine, but also methylates N3 adenine and O6 guanine residues [80].

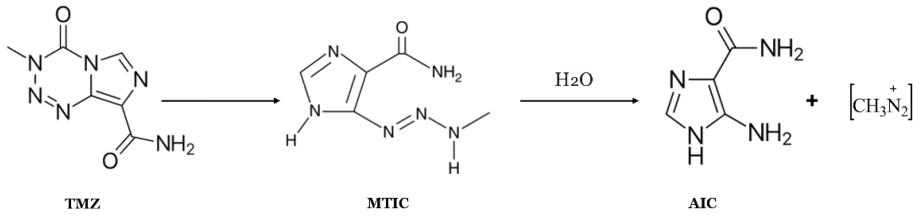

Figure 3. Structure and activation pathway of Temozolomide.

When the methyldiazonium cation methylates the DNA at the O6 position of the guanine, it results in the formation of the O6-methylguanine (O6-MeG) lesion. This lesion is harmful because it is carcinogenic, mutagenic and interferes with the normal functioning of DNA. As a defense mechanism, the enzyme methylguanine-DNA methyltransferase (MGMT) is activated, which repairs the lesion by removing the methyl group from O6-MeG and restoring the guanine to its normal state [81]. However, the promoter region of the MGMT gene is hypermethylated in around 30% to 60% of glioblastoma patients, which generally leads to suppression of gene expression, meaning that the cell produces less or no MGMT enzyme. Thus, the O6-MeG lesion is not repaired, leading to incorrect pairing with thymine instead of cytosine [81]. This error is detected by the DNA mismatch repair (MMR) system; however, MMR only removes the thymine from the new DNA strand, leaving the O6-MeG on the parental strand [81]. As a result, the thymine is repeatedly reinserted and removed in a cycle, causing persistent breaks in the DNA chain [81]. The accumulation of these breaks leads to the collapse of replication forks, structures necessary for DNA replication, triggering an arrest in the cell cycle in the G2/M phase leading to persistent DNA damage and replicative stress eventually inducing apoptosis [80, 81] (Fig 4).

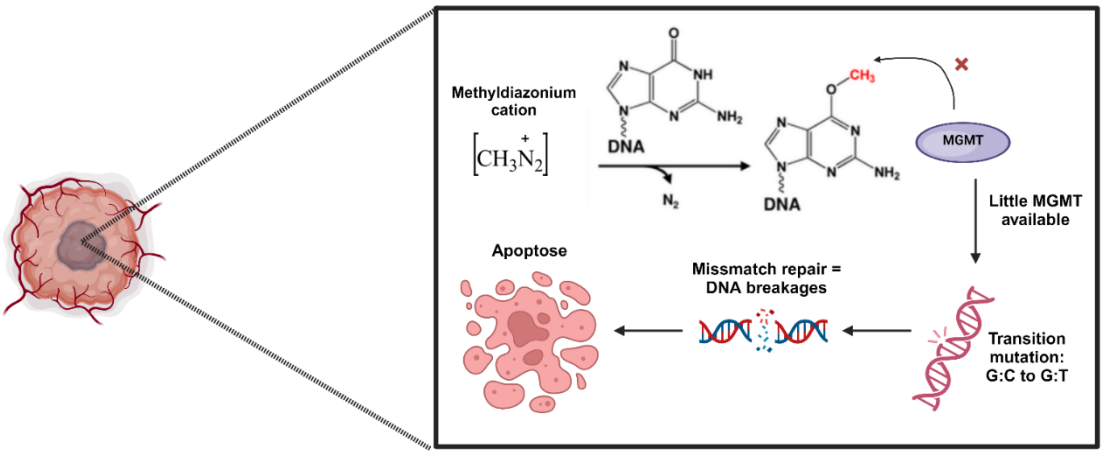

Figure 4. Mechanism of action of temozolomide (made in biorender.com).

1.2.2.1. Mechanisms of TMZ resistance

Tumors initially sensitive to chemotherapy often develop resistance – acquired resistance [82]. This process occurs in a similar way to Darwinian evolution, in which chemotherapy acts as a selective pressure on tumor cells, which are very diverse, allowing those with mutations or characteristics that give them resistance to survive the treatment [82, 83]. Although most tumor cells are destroyed by chemotherapy, the few resistant cells manage to survive, proliferate and give rise to a new tumor, now composed predominantly of cells that no longer respond to treatment, since the environment with the chemotherapeutic agent favors the selection and growth of these resistant cells [83].

Although TMZ is the main drug for treating gliomas, inherent and acquired resistance led to treatment failure [83]. This resistance is caused by various factors such as: the activity of DNA repair enzymes (MGMT and MDR); overexpression of the epidermal growth factor receptor (EGFR); galectin-1, murine double minute 2 (Mdm2); p53 and mutations in the phosphatase and tensin homologue (PTEN) [84].

1.2.2.1.1. O^6-Methylguanine DNA methyltransferase (MGMT)

The efficacy of TMZ depends on the DNA methylation status of the O6-methylguanine DNA methyltransferase (MGMT), which has been identified as a prognostic biomarker in glioblastoma patients [85]. The MGMT gene is located on chromosome 10q26 and is made up of five exons. Its promoter region is largely covered by a 762 base pair CpG island, which contains 98 CpG dinucleotides and covers a large part of the promoter region and the first exon of the gene [86]. Clinical studies revealed that glioblastoma patients with hypermethylated MGMT promoter have a better response to TMZ treatment and a significantly improved overall survival [87]. The expression level of MGMT depends on the methylation level of its promoter region [87]. When glioblastoma patients lack the methylated MGMT promoter zone it leads to high levels of MGMT in the cells that repair the DNA damage caused by TMZ, preventing the drug from inducing cytotoxicity. As a result, the cells become resistant to TMZ, reducing its therapeutic efficacy [88]. One way to overcome TMZ resistance is to epigenetically silence the MGMT gene, this can be achieved by promoter methylation thereby reducing its DNA repair activity.

1.2.2.1.2. Multidrug resistance (MDR)

MDR occurs due to the overexpression of certain proteins that remove chemotherapeutic agents from cells, limiting their concentration and reducing their therapeutic effect [89]. The group of proteins that are associated with MDR are the protein transporters of the ATP-binding cassette (ABC) family of drugs [89]. This family is encoded by 49 genes and is subdivided into 7 subfamilies [89]. In glioblastoma, the genes from three subfamilies are predominantly expressed: ABCB, ABCC, and ABCG [90].

The best studied of the ABCB family is the ABCB1 protein (member 1 of subfamily B of the ATP-binding cassette) (P-gp, P-glycoprotein) [90]. P-gp is expressed in the endothelial cells of the BBB capillaries and excretes drugs from the cerebrospinal fluid and plasma [90]. The regulation of the gene that gives rise to the overexpression of this protein is carried out by two signaling pathways: MAPK/ERK1/2 and PI3K/AKT/NF-κB [89]. These pathways are hyperactivated (due to mutations or stimuli in the tumor microenvironment), leading to an increase in the transcription and activity of ABCB1, decreasing the intracellular concentration of TMZ below therapeutic levels, limiting its effect [89].

1.2.2.1.3. DNA base excision repair (BER) pathway

BER is a DNA repair pathway that acts as a cellular defense mechanism to prevent and/or repair damage to DNA bases including base modifications, abasic sites, as well as single-strand breaks [91]. Alkylpurine–DNA–N-glycosylase (APNG), also known as 3-methyladenine-DNA glycosylase, is a base excision repair enzyme involved in the BER pathway, which repairs the cytotoxic lesions N^3-methyladenine and N^7-methylguanine, caused by temozolomide decreasing the therapeutic effect [92]. Studies show that TMZ-resistant GBM cell lines often express both APNG and MGMT, and down-regulation of either enzyme sensitizes the cells to TMZ [92]. Furthermore, introducing APNG into TMZ-sensitive cells conferred resistance, whereas catalytically inactive APNG mutants did not [92].

1.2.2.1.4. Epidermal Growth Factor Receptor (EGFR) and galectin-1

EGFR is a transmembrane tyrosine kinase receptor that regulates key cellular processes, including proliferation, survival and differentiation and is frequently expressed at elevated levels in different forms of cancer [93]. In GBM, EGFR is often amplified or mutated, contributing to tumor aggressiveness and resistance to treatment [94]. The EGFR family contains four members: Designated EGFR (known as ErbB1/HER1), ErbB2 (HER2/Neu), ErbB3 (HER3) and ErbB4 (HER4) [95]. The EGFR pathway is activated by more than one mechanism, such as increased production or overexpression of the ligand, mutation of the receptor or impaired inactivation. EGFR can activate a variety of signal transduction pathways simultaneously [95]. One of the most frequently studied pathways is the recruitment and activation of the phosphatidylinositol-3-kinase (PI3K) signaling network, which is responsible for tumor growth caused by the downstream activation of AKT and mTOR proteins [95]. The RAS/RAF/MEK/ERK pathway is another downstream signaling pathway activated by EGFR [96]. EGFR activates the RAS protein, which stimulates the RAF protein, initiating a phosphorylation cascade that activates the ERK pathway [96]. Once activated, ERK translocates to the nucleus, where it regulates the expression of genes that promote cell proliferation and differentiation [96]. The hyperactivation of the RAS/RAF/MEK/ERK pathway leads to uncontrolled cell growth and prevents apoptosis, contributing to tumor progression and resistance to TMZ [96]. Galectin-1 is a carbohydrate-binding protein (lectin) that plays a role in cell proliferation, apoptosis, immune evasion and tumor progression [97]. Galectin-1 complements the pro-survival effects of EGFR by modulating the tumor microenvironment and reinforcing cell survival pathways [97]. Galectin-1 also activates PI3K/AKT and MEK/ERK signaling through interactions with H-Ras and K-Ras, reflecting some of the downstream effects of EGFR [98]. This dual activation of key survival pathways by both galectin-1 and EGFR creates a synergistic effect in which tumor cells receive pro-survival signals, making them more resistant to the cytotoxic effects of TMZ [99].

1.2.2.1.5. p53 and Mdm2

p53, often referred to as the "guardian of the genome," is a tumor suppressor protein that regulates the cell cycle and prevents the propagation of genetically damaged cells [100]. It functions primarily as a transcription factor that activates the expression of various genes involved in cell cycle arrest, DNA repair, and apoptosis [100]. When DNA is damaged, p53 activates genes that promote cell cycle arrest for DNA repair, or initiates apoptosis if the damage is irreparable [101]. TMZ mainly induces O6-meG lesions in DNA, leading to replication errors [102]. The p53 pathway when functional leads to apoptosis of these cells, however, in glioblastoma the p53 gene is often mutated, resulting in the loss of p53 function [103]. Mutant p53 protein can no longer effectively induce cell cycle arrest or apoptosis, allowing GBM cells to escape the cytotoxic effects of TMZ and leading to greater resistance [104, 105]. The availability of p53 is often reduced in GBM because it binds to the oncoprotein MDM2, which accumulates in high concentrations in tumor cells [106]. MDM2 is an E3 ubiquitin ligase that is overexpressed in glioblastoma in most cases, so even if p53 is functional, it ends up having no effect, as it ends up being degraded by MDM2 reducing the therapeutic effect of TMZ [107].

1.2.2.1.6. Phosphatase and Tensin Homolog (PTEN)

Gliomas are naturally resistance to apoptosis because of phosphate and tensin homologue on chromosome 10 (PTEN) tumor suppressor mutation and constitutively active Akt/PI3K/mTOR/NF-kB signaling [108]. Under normal conditions, PTEN dephosphorylates PIP3 (phosphatidylinositol (3,4,5)-trisphosphate), which inhibits the activation of AKT [109]. When PTEN is lost or mutated, this inhibitory effect is removed, leading to hyperactivation of the PI3K/AKT signaling pathway which leads GBM cells to avoid TMZ-induced cell death by inhibiting pro-apoptotic factors [110]. When activated, AKT phosphorylates and inactivates pro-apoptotic proteins such as BAD and caspase-9, which are responsible for initiating apoptosis [111]. This allows cells to avoid programmed cell death even when they experience stress or DNA damage, a key mechanism in cancer cells' resistance to therapies like TMZ [111].

1.2.2.1.7. Blood-Brain Barrier (BBB)

The BBB is a highly selective and protective barrier that separates the brain's extracellular fluid from the circulating blood, maintaining a stable environment for proper neural function. It is formed mainly by endothelial cells lining the cerebral capillaries, which are connected by tight junctions that restrict the movement of substances (Figure 5) [112]. These cells are supported by a basement membrane and astrocyte end-feet, which increase the integrity of the barrier and regulate signaling [112]. The BBB prevents harmful substances, pathogens and toxins from entering the brain, while allowing nutrients, gases and waste products to pass through selectively [113]. The blood-brain barrier ~~(BBB),~~ although essential for protecting the brain, represents a major obstacle for the pharmacotherapy of diseases of the central nervous system (CNS) [113]. It

is estimated that more than 98% of small molecule drugs and all macromolecular drugs are excluded from access to the brain [113]. This is due to the presence of tight junctions between endothelial cells, which limit the passage of substances, allowing only the passive diffusion of fat-soluble drugs [113]. The tight junctions (Figure 5) permit only the passive diffusion of lipid-soluble drugs with a molecular weight below 400-600 Da [113]. In addition to the physical barriers, specific mechanisms facilitate the transport of essential substances like amino acids and glucose into the brain while ensuring the removal of excess compounds from the CNS [113]. As a result, insufficient administration of drugs into brain tissue compromises therapeutic efficacy and can aggravate side effects due to the accumulation of drugs in other organs and tissues [113].

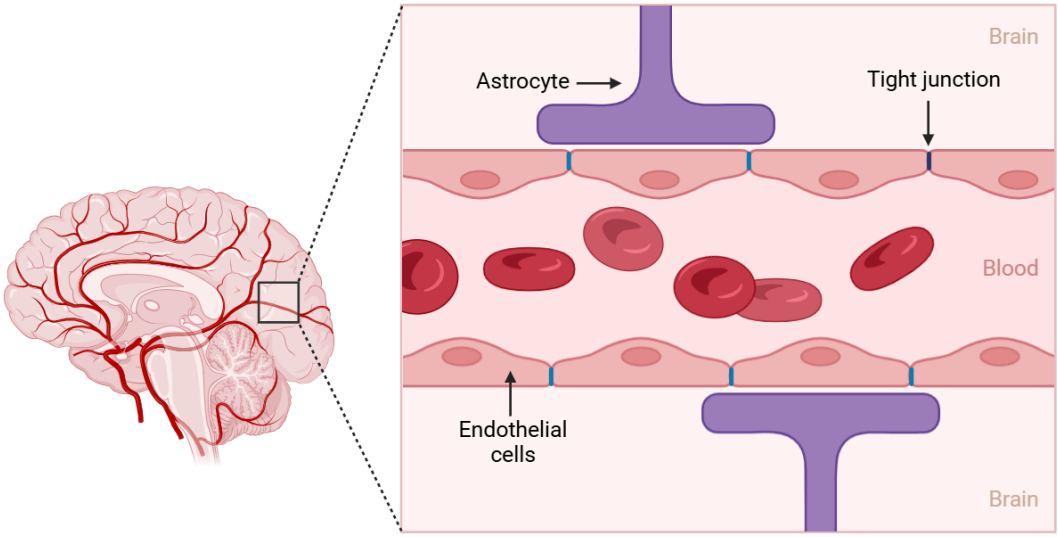

Figure 5. Structure of the blood-brain barrier (BBB).

Although TMZ has the ability to cross the BBB due to its size of 194 Da, its efficacy is limited by the incomplete penetration of the dose into the brain [114]. A significant part of the drug does not reach the brain parenchyma, as TMZ is unstable and rapidly degrades into its active metabolite, MTIC, which cannot effectively cross the BBB [114]. To overcome these limitations, various TMZ administration strategies have been investigated, such as chemical modifications, encapsulation in controlled release systems and alternative administration approaches [114].

1.3. Gene therapy

Conventional therapies may slightly improve the results of cancer treatment, but in the long term they are ineffective due to metastasis and tumor recurrence, and the fact that they also affect normal cells and affect the patient's immune system [115, 116]. Gene therapy has emerged as a promising tool allied to conventional therapies to improve cancer therapy [117]. Gene therapy is described as the process used to treat or improve a patient's health by genetically modifying their

cells, which involves introducing therapeutic genetic material such as DNA or RNA, into the cell nucleus [118]. The aim is to correct the loss of function caused by a mutation or to restore the expression of a deficient gene to appropriate physiological levels [118]. There are several strategies for delivering gene therapy, with viral and non-viral vectors being the most prominent methods [119].

Gene therapy has shown promise in treating various diseases, such as hemoglobinopathies and immunodeficiencies viral infections by modifying or replacing single genes [120]. In cancer treatment, gene therapy is being explored to introduce genes or blocking genes that cause tumor growth [121]. Gene therapy has also made progress in fighting viral infections such as HIV by using genes that block virus replication or stimulate the immune system [122].

Despite the promises, gene therapy faces several challenges including efficient cell-to-cell delivery, long term gene expression, stimulation of immune reactions and ensuring the safety of genetic modification, however continued advances in CRISPR-Cas9 gene editing technology along with improvements in gene delivery vectors and manipulation have been made [123].

1.3.1. Viral vectors

Viral vectors were the first vectors to be discovered and are today one of the most widely used tools in gene therapy due to their high efficiency in introducing genetic material into target cells [124]. Viruses are naturally adapt at entering cells and introducing their genetic material, which makes them ideal candidates for gene therapy applications [125]. In viral vectors, the harmful or pathogenic genes of the virus are removed and replaced with therapeutic genes [125]. Although effective in delivering genetic material, they have several negative effects in gene therapy as the body's immune response can recognize the vector as an invader, resulting in adverse reactions such as fever or anaphylactic shock [126]. In addition, vectors that integrate genetic material into the genome can cause insertional mutagenesis [126]. The most common viral vectors include adenoviruses, adeno-associated viruses (AAV) and retroviruses (Figure 6) [124].

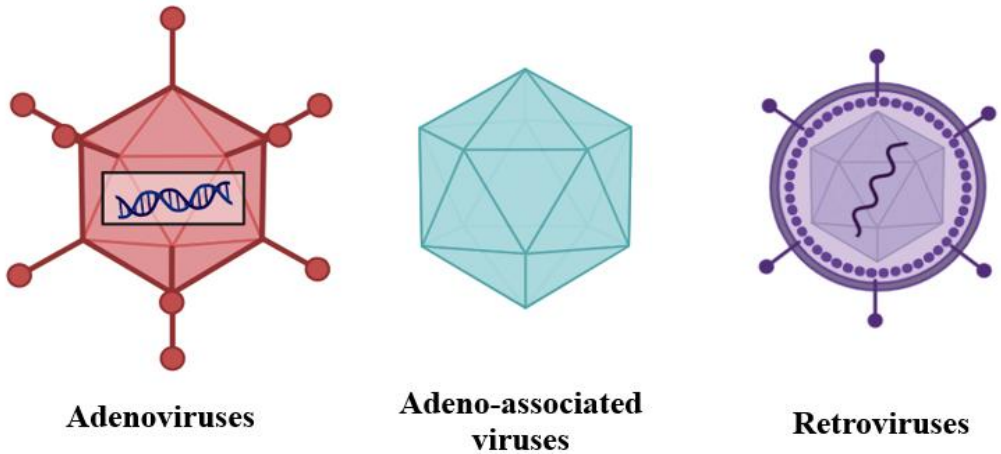

Figure 6. Examples of viral vectors used in gene therapy (made in biorender.com).

Adenoviruses are non-enveloped, double-stranded DNA viruses belonging to the family *Adenoviridae* [127]. They were first discovered in the adenoid tissues of humans [127]. The virus is non-enveloped and has an icosahedral-shaped protein coat (capsid) that protects its DNA [127]. Adenoviral vectors are useful in gene therapy due to their ability to efficiently deliver genetic material to various types of cells [128]. Although the viruses are altered, they are naturally immunogenic, which means that the host's immune system recognizes them as foreign and begins an aggressive defense [129]. This can lead to significant inflammation at the site of administration and even system-wide immune reactions [130]. If the body quickly eliminates the virus, this reduces the effectiveness of gene therapy [130].

Adeno-associated viruses (AAVs) are small, non-enveloped viruses belonging to the *Parvoviridae* family, initially discovered as contaminants in adenovirus preparations [131]. They are advantageous for gene therapy due to their safety profile, low immunogenicity, and ability to deliver therapeutic genes to a wide range of tissues, including muscle, liver, and the central nervous system, without causing significant disease or inflammation [132].However, their packaging capacity is relatively small, typically accommodating genes up to about 4.9 kilobases, which restricts their use for larger therapeutic genes [133]. Additionally, pre-existing immunity to AAVs in some individuals, due to natural exposure to the virus, can significantly reduce the efficacy of the treatment [133].

Retroviruses are a class of RNA viruses characterized by their replication process, which involves the reverse transcription of their RNA genome into DNA [134]. This DNA is then integrated into the host cell's genome, allowing the virus to replicate as the host cell divides. They can effectively deliver genes into dividing cells and have a high integration efficiency, resulting in stable and long-lasting gene expression [134, 135]. However the risk of insertional mutagenesis in which the integration of viral DNA disrupts essential genes or regulatory elements can lead to adverse effects, including the development of cancers [136].

1.3.2. Non-Viral vectors

Non-viral vectors have been widely studied for gene delivery because they have low cytotoxicity, immunogenicity and mutagenesis [137]. However, they do not have ideal characteristics, and their lower gene transfection efficiency and specificity compared to viral vectors is a challenge for their clinical application [137]. These vectors are usually attached to transport delivery vehicles such as polymers, lipids, liposomes, inorganic particles and combinations of different types [137]. The delivery of non-viral vectors can use physical forces (microinjection, needle injection, needle-free jet injection, gene gun, electroporation, sonoporation, hydroporation, magnetofection and laser irradiation) to allow the nucleic acid to cross the cell membrane and reach the cell without any carrier agent [138]. Plasmid DNA has been widely studied in this field due to its modular structure, which enables straightforward molecular cloning, making it easy to modify and design for therapeutic purposes [139].

1.3.3. Plasmid DNA (pDNA)

pDNA expression vectors are essential tools for all types of non-viral gene delivery [140]. Unlike viral vectors, pDNA does not carry the risk of viral integration or immune responses, making it a safer alternative for gene delivery [141]. It can be engineered to include therapeutic genes, regulatory elements, and sequences that optimize gene expression, allowing for tailored design based on specific therapeutic needs [142]. Plasmids are extra-chromosomal small circular DNAs that are capable of replicating independently of the host, their size ranging from 0.8 to 200 kbp [143].

Plasmids are produced in bacteria, which means that, alongside their therapeutic genes, they must include a bacterial origin of replication and a selection marker, typically an antibiotic resistance gene, to ensure their maintenance during bacterial growth [144]. Achieving stable plasmid structure and efficient replication in bacterial cultures is essential for high-quality plasmid DNA production [144].

pDNA can exist in five distinct isoforms, each differing in its structural configuration, the supercoiled, open-circular, linear, relaxed circular, and the supercoiled denatured conformation. [145, 146]. The most common isoform is the supercoiled form, in which the DNA is coiled into a compact, circular structure, which is generally preferred in gene therapy due to its stability and efficient transfection into cells [147]. Another form is the open circular, in which one of the DNA strands has been cut, resulting in a more relaxed structure; this form is less efficient in gene delivery and is often considered a contaminant during plasmid purification [148]. A third isoform is the linear form, which occurs when both DNA strands are cut; although it can integrate more easily into the host genome, it is generally less stable and more susceptible to degradation [149]. The relaxed circular form has an uncoiled structure, and the supercoiled denatured conformation consists of multiple plasmid molecules interconnected as a chain; this form often arises during plasmid production in bacteria and is undesirable due to difficulties in separation and purification [146].

1.4. Nanoparticle-Based Drug Delivery Systems

The delivery of pDNA into cells is a challenge in gene therapy due to its inability to cross the eukaryotic cell membrane barrier and reach the nucleus, which has led to the development of various delivery systems [150]. For therapeutic use, these delivery systems need to have an appropriate size, the ability to encapsulate large amounts of DNA, and provide protection against enzymatic degradation, they must also effectively evade the innate immune system and ensure that the therapeutic payload is released in a controlled, sustained manner [151, 152]. They also must be biocompatible, have minimal side-effect profile (such as low inflammation risk), and efficient biodistribution throughout the body [151, 152] .

1.4.1. Types of delivery systems

Delivery systems are designed to specifically target diseased cells, enabling direct treatment of those cells. This targeted approach enhances therapeutic efficacy while minimizing side effects, ultimately leading to better overall health outcomes [153]. The delivery systems can be broadly categorized into 2 major categories: organic and inorganic (Figure 7) [154-156].

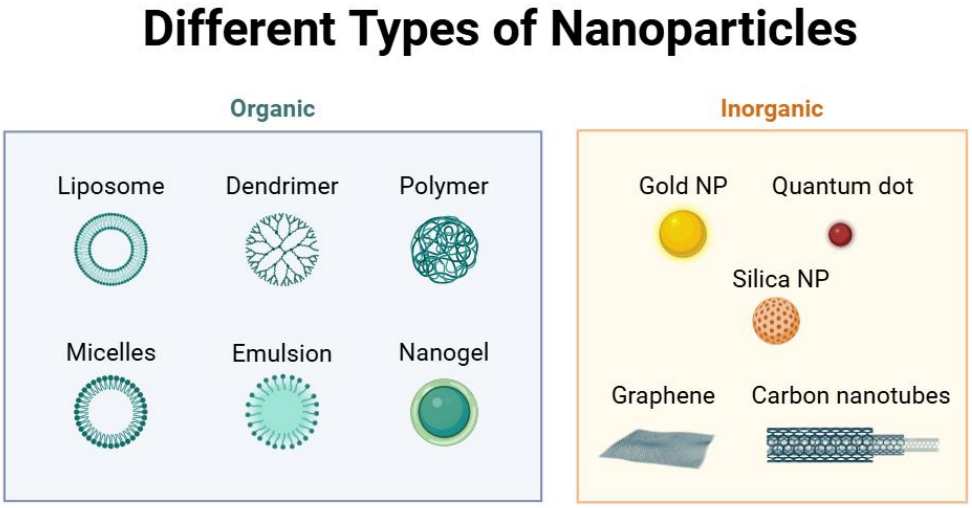

Figure 7. Different types of nanoparticles are divided in 3 major categories: organic, inorganic and carbon-based (made in biorender.com).

Within the group of organic transport vectors we have, for example, lipid-based vectors such as liposomes, which seem to be an almost ideal drug transport system, since their morphology is like the one displayed by cell membranes and due to their ability to incorporate various substances [157]. Liposomes are spherical vesicles consisting of one or more phospholipid bilayers surrounding an aqueous core [157]. Due to their structure, they can encapsulate both hydrophilic and hydrophobic substances, making them versatile carriers for drug delivery and gene therapy [157]. The hydrophilic drugs are held in the aqueous interior, while lipophilic or hydrophobic drugs are incorporated into the lipid bilayers [157]. This dual ability allows liposomes to protect their cargo from degradation and enhance the stability of otherwise unstable therapeutic agents [157]. Dendrimers are highly branched, tree-shaped molecules with internal cavities that can encapsulate drugs and surface groups that can be modified for targeted administration, offering precise control of drug size and release [158]. Micelles are made up of amphiphilic molecules that self-assemble into a core-shell structure, in which the hydrophobic core can transport water-insoluble drugs, while the hydrophilic shell helps disperse them in aqueous environments [158]. Polymeric nanoparticles are made from biodegradable polymers such as PLGA, offering a sustained and controlled release of drugs and the possibility of modifying the surface to suit their orientation [159]. Emulsions, especially nanoemulsions, are mixtures of oil and water stabilized by surfactants, allowing the release of hydrophobic drugs with improved bioavailability [160]. Nanogels are hydrogel-based carriers that can encapsulate hydrophilic and hydrophobic drugs,

and their high-water content allows for biocompatibility and reaction to environmental changes such as pH or temperature, allowing for the controlled release of drugs [160].

Inorganic delivery systems, such as gold nanoparticles, quantum dots, and silica nanoparticles, have gained significant attention in drug delivery and biomedical applications due to their unique properties and versatility [161-163]. Gold nanoparticles (AuNPs) can be biocompatible and have unique optical and electronic properties, their surfaces can be functionalized with drugs, antibodies, or targeting ligands, allowing for precise delivery and minimizing off-target effects [161]. Quantum dots are semiconductor nanocrystals that emit fluorescence when excited, their tunable optical properties allow for multiplexing in imaging applications, and they can be conjugated with drugs for targeted therapy, especially in cancer treatment [162]. Silica nanoparticles, particularly mesoporous silica nanoparticles (MSNs), offer a high surface area and tunable pore sizes, making them ideal for loading a variety of therapeutic agents [163]. They are chemically stable, and their surface can be modified to enhance biocompatibility and enable targeted delivery [164]. Graphene is a single layer of carbon atoms arranged in a two-dimensional honeycomb lattice, which provides exceptional electrical conductivity, high surface area, and mechanical strength [165]. Graphene's surface can be easily functionalized to enhance biocompatibility and target specific cells, allowing for efficient drug delivery and controlled release [166]. Furthermore, its ability to form stable dispersions in biological fluids facilitates the transport of loaded therapeutic agents within the body [166]. Carbon nanotubes (CNTs), on the other hand, are cylindrical structures composed of rolled-up sheets of graphene. CNTs possess remarkable mechanical strength, electrical conductivity, and a high aspect ratio, which allows them to effectively penetrate cell membranes and deliver payloads directly into cells [167]. Like graphene, CNTs can be functionalized to improve solubility and biocompatibility and to attach therapeutic agents, enabling targeted delivery to specific tissues or cells [168].

1.4.2. Cell Penetrating Peptides

Cell-penetrating peptides (CPPs) are a class of short peptides, usually between 5 and 30 amino acids, with the ability to facilitate the delivery of various bioactive molecules, including proteins, nucleic acids and small drugs, across cell membranes [169]. These peptides are rich in basic amino acids such as arginine and lysine, which confer a positive charge that increases their interaction with negatively charged cell membranes [169].

CPPs can be classified into two main types: basic peptides, which rely on electrostatic interactions to enter cells, and hydrophobic peptides, which promote membrane fusion [169]. Their cellular uptake mechanisms can vary, including direct translocation through lipid bilayers or the induction of endocytosis, which allows them to efficiently transport larger loads [169]. CPPs can be modified to improve stability and bioavailability, and their surfaces can be modified with targeting ligands to increase specificity towards certain cell types [170].

CPPs serve as effective transporters due to their ability to facilitate the movement of macromolecular cargoes, such as polypeptides, nanoparticles, and oligonucleotides, across the

cell membrane [171]. While the precise mechanisms of cellular uptake are still being explored, several proposed methods include direct penetration, endocytosis, and the formation of transient structures that aid translocation [171]. CPPs exhibit a diverse array of physicochemical properties and structures, and they are also referred to as protein transduction domains (PTDs) or Trojan peptides [171]. Their endogenous nature, or similarity to naturally occurring proteins, enhances their suitability for *in vivo* applications, as they are generally biocompatible and non-immunogenic [171].

1.4.3. WRAP5

WRAP5 is a cell-penetrating peptide that consists of 15 amino acids, characterized by a sequence rich in tryptophan (W), arginine (R), and leucine (L) residues [172]. With a net positive charge of +5, WRAP5 is capable of self-assembling into nanoparticles with diameters ranging from 80 to 100 nm[172]. This peptide is designed to efficiently complex nucleic acids, forming stable nano-systems that facilitate cellular transfection [172]. The mechanism by which WRAP5 mediates cellular uptake is believed to involve direct translocation through the cell membrane or endocytosis, followed by a swift escape from the endosomal compartment [172]. Additionally, the surface of WRAP5 nanoparticles can be functionalized with targeting ligands, enhancing the selectivity and efficacy of CPP-based delivery systems in therapeutic applications [172].

1.5. Tumor Targeting: Serum Albumin

The coating of nanoparticles with serum albumin is emerging as a promising strategy for the administration of specific drugs in glioblastoma therapy [173]. Derived from bovine blood, BSA is a protein widely used in various biotechnological applications due to its excellent biocompatibility, stability and low immunogenicity, which makes it an ideal candidate for coating nanoparticles [174]. When nanoparticles are coated with BSA, they gain a biocompatible “shell” that increases their stability and allows specific targeting of cancer cells, including those associated with glioblastoma [175]. Glioblastoma presents challenge due to its location in the brain and the presence of the blood-brain barrier [175]. However, BSA-coated nanoparticles can be engineered to cross this barrier, improving their ability to effectively target tumor sites [175]. In addition, BSA interacts with various receptors and cell surface proteins on glioblastoma cells, including albumin-binding proteins that are frequently present on these cancer cells [176]. This intrinsic interaction facilitates the binding and internalization of BSA-coated nanoparticles by glioblastoma cells [176].

BSA is widely used in in vitro studies due to its low cost and high availability, making it a practical choice for early-stage research and large-scale assays [177]. Despite being derived from bovines, BSA shares significant structural and functional similarities with human serum albumin (HSA), with a sequence homology of approximately 76%, allowing it to mimic many of HSA’s roles in experimental setups [177]. However, in pharmaceutical formulations intended for human use, HSA is preferred because of its species-specific compatibility and reduced risk of immunogenic

reactions [178]. While BSA is invaluable in research for its affordability, HSA's physiological relevance makes it essential for therapeutic applications in human medicine.

1.5.1. Enhanced permeability and retention (EPR) effect

Albumin-containing nanoparticles can accumulate in solid tumors via passive and active transport mechanisms, increasing its effectiveness as a therapeutic vehicle [179]. One of the main mechanisms is the EPR—effect, which allows albumin-bound nanoparticles to passively accumulate in tumors [179]. The EPR effect occurs due to the presence of dilated and leaky blood vessel walls in tumors, which facilitates the extravasation of nanocarriers between 20 and 250 nm in size from the bloodstream into the tumor's interstitial space (Figure 8) [179]. In addition, poor lymphatic drainage in tumor tissues further aggravates the accumulation of these nanoparticles, since fluids and other substances cannot effectively leave the tumor, leading to an increase in the concentration of leaky nanoparticles in the tumor environment [179].

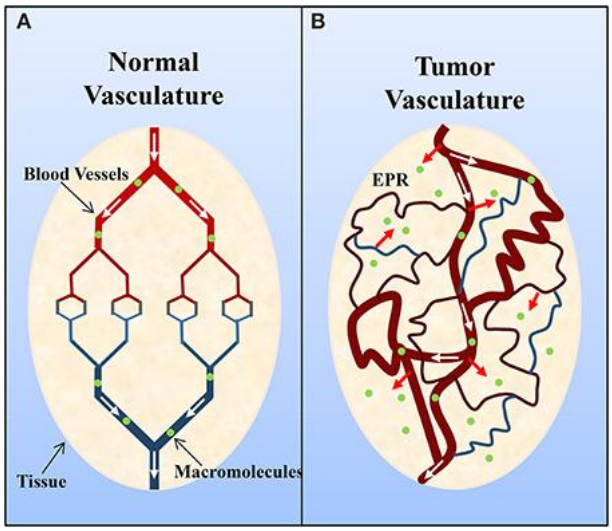

Figure 8. Schematic representation of (A) normal and (B) tumor vasculature (adapted from [170]).

In addition, albumin from these nanoparticles can interact with albumin-binding glycoproteins, such as gp60, which are expressed on the surface of endothelial cells in the tumor vasculature [179]. This binding occurs with high affinity and can trigger the internalization of the albumin-bound nanoparticles by the cancer cells, facilitating their targeted administration [179]. Once internalized, the drug-loaded albumin nanoparticles can undergo intracellular transport and release their therapeutic cargo into the tumour tissue [179]. This dual mechanism of accumulation and targeted release increases the potential for better therapeutic results in cancer treatment, particularly in difficult environments such as glioblastoma, where effective drug delivery is critical [179].

1.5.2. Secreted protein, acidic and rich in cysteine (SPARC) receptors

SPARC is a multifunctional glycoprotein recognized for its involvement in biological processes such as cell-matrix interactions, extracellular matrix (ECM) remodeling and tumor progression [180]. Since tumor cells, including gliomas, proliferate abnormally quickly, they consume a significant amount of energy to sustain this growth, requiring various nutrients, including albumin [180]. Although albumin is typically prevented from entering the brain, the rapid proliferation of highly metabolically active tumors leads to nutrient deprivation, prompting tumor cells to increase their uptake of albumin for use as an amino acid and energy source [180]. To facilitate albumin absorption in glioma tissues, SPARC is over-expressed compared to surrounding nerve and vascular endothelial cells [180]. This overexpression allows albumin to be introduced into gliomas in large quantities through endocytosis by tumor cells. SPARC is an extracellular glycoprotein that is abnormally overexpressed in solid cancers, including brain tumors, acting as a promoter of tumor proliferation and metastasis [180]. Furthermore, although SPARC is expressed at low levels in a normal adult brain, it is significantly overexpressed in all grades of glioblastoma, particularly in regions where metastasis is actively occurring [180]. This interaction between SPARC and albumin uptake highlights the potential for using SPARC to improve the delivery of drug-loaded BSA-coated nanoparticles into the tumor microenvironment [180].

As shown in Figure 9, the binding of BSA-coated nanoparticles to the 60 kDa glycoprotein (Gp60) on endothelial cells triggers the activation of caveolin-1, a pivotal protein essential for the formation of caveolae, specialized invaginations in the cell membrane that mediate transport across endothelial cells [174]. This process enables the transcytosis of nanoparticles across the endothelial cell membrane, preserving their structural integrity and protecting them from enzymatic degradation during transit [174]. SPARC exhibits a high affinity for albumin molecules present in these nanoparticles [174]. The tumor microenvironment, frequently characterized by a defective lymphatic drainage system and highly permeable blood vessels, amplifies this interaction [174]. The binding between SPARC and albumin enhances nanoparticle retention near tumor cells, creating a localized and sustained drug delivery mechanism [174]. Furthermore, SPARC significantly contributes to extracellular matrix remodeling, a process that increases tissue permeability [174]. This enhanced permeability facilitates deeper penetration of nanoparticles into tumor tissue, optimizing their distribution and maximizing the concentration of therapeutic agents directly at the site of action [174]. Such mechanisms collectively improve the efficiency of drug delivery, potentially elevating therapeutic outcomes by targeting tumor cells with greater precision [174].

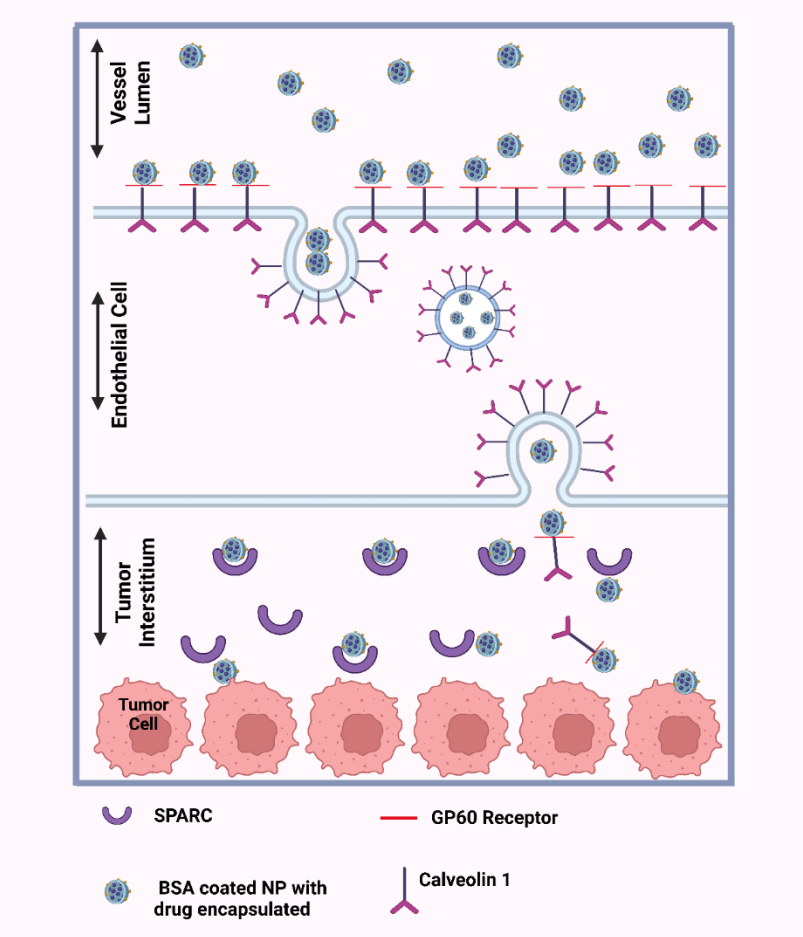

Figure 9. Illustration on BSA coated NPs internalization in a tumor (adapted from [172] and made with biorender.com).

1.6. Design of experiments (DoE) to optimize drug delivery systems

DoE is a mathematical modeling approach developed in the early 20th century by Sir Ronald A. Fisher who introduced the idea of integrating statistical analysis into the planning stages of research rather than applying it solely after experimentation [181]. DoE is an essential method in the application of Quality by Design (QbD) and is widely used in research and industrial processes [181].

QbD is a scientific approach that emerged to create guidelines for drug approval, to establish strict specifications to guarantee product quality [182]. One of the principles of QbD is that product quality can only be guaranteed if the critical factors influencing product variability are understood and properly eliminated or controlled within a previously established design space [182]. This approach makes it possible not only to analyze the factors studied (independent variables) and optimize the responses (dependent variables) of the evaluation, but also to present, in addition to the p-values of the input variables, the degree of impact on the responses in linear, quadratic and

fully quadratic analyses [182]. Studies show that the QbD methodology incorporates the use of DoE as a tool for the structured and controlled improvement of various nanocarriers such as solid lipid nanoparticles, liposomes, gold nanoparticles, polymeric micelles, etc [183-188].

DoE tools are statistical methods that help to understand how the inputs (alone and in combination) affect the outputs (responses) [189]. Inputs are the variables that can be controlled during the formulation of nanocarriers; these can include material concentrations, processing conditions (such as temperature and time) and physical characteristics (such as particle size or surface charge) [189]. The outputs refer to the results of interest, which may include the drug encapsulation efficiency, release profiles, stability and biocompatibility of the nanocarriers [189].

The choice of DoE methods can significantly affect the efficiency and effectiveness of the experimental process [182]. There are two main groups of methods that can be used such as Screening Designs (Plackett-Burman Design, Fractional Factorial Design, Full Factorial Design) and Response Surface Methodology (RSM) (Box-Behnken Design (BBD), Doehlert Design, Central Composite Design (CCD)[182]. Screening designs are methods used to identify the most significant factors affecting the response variables [190]. The Plackett-Burman design is a two-level factorial design that allows the selection of many factors with a minimum number of experiments [190]. Fractional Factorial Design examines only a subset of the possible combinations of factors, which makes it more resource-efficient than a full factorial design [190]. Response surface methodology (RSM) is used to optimize the chosen key inputs and outputs and explore the relationships between them in more depth [190]. The Box-Behnken Design (BBD) is a three-level design that is particularly useful for constructing a second-order response surface [190].The Doehlert Design is a less common but effective design for response surface methodology that allows multiple factors to be explored at varying levels [190]. The Central Composite Design (CCD), showed in Figure 10, is the most popular class of second order design, and it is widely used to build a quadratic model for the response variable without the need for a full three-level factorial experiment [191]. It comprises 2k full factorial points, where k is the number of independent variables, allowing for the exploration of all possible combinations of factor levels [191]. In addition, the design includes 2k axial or star points positioned at a distance $(\pm\alpha, 0,\ldots, 0)$, $(0,\pm\alpha,\ldots , 0)$, from the center along each axis, enhancing the ability to capture curvature in the response surface (Figure 10) [191]. This structure is further supplemented by one or more center points, represented by $(0,0,\ldots,0)$ which provide estimates of experimental error and assess response variability [191]. The combination of factorial, axial, and center points in CCD enables a comprehensive exploration of the design space while minimizing the number of required experimental runs, thereby increasing efficiency [191]. Moreover, the axial points facilitate the identification of nonlinear relationships between factors and responses, resulting in robust modeling capabilities [191].

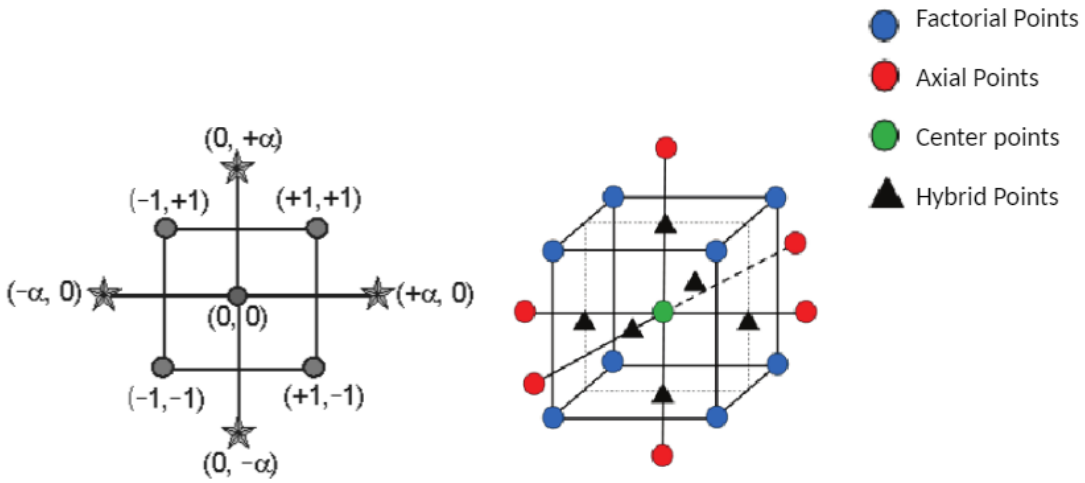

Figure 10. Central Composite Design (CCD) (adapted from [184]).

The use of DoE in the development of nanocarriers offers several advantages, as it increases efficiency by simplifying the experimental process and reducing the number of trials needed to obtain reliable data, thus saving time and resources [182]. In addition, the systematic study of multiple factors and their interactions leads to the development of robust nanocarriers that work consistently under various conditions [182]. DoE thus allows the creation of mathematical models that describe the relationships between factors and responses, providing valuable insights that facilitates and promotes the design and optimization of nanocarriers [182].

Chapter 2- Aim of the thesis

The main aim of this thesis is to develop and optimize BSA-coated TMZ-WRAP5/p53 nanocomplexes using a design of experiments approach to improve their efficacy as a targeted co-delivery system for glioblastoma.

This research focuses on identifying the ideal formulation parameters to improve the size, surface charge, and pDNA complexation capacity of the nanocomplexes.

In addition, the research seeks to effectively coat the nanocomplexes with BSA in order to increase the biocompatibility, stability and specificity of the nanocomplexes, making them more suitable for the treatment of glioblastoma.

Using the ideal formulation determined by the DoE, the aim is to demonstrate through in vitro experiments that these nanocomplexes possess favorable properties for potential clinical translation against glioblastoma. This includes evaluating their biocompatibility, cytotoxicity, hemocompatibility, co-delivery efficiency, and the potential synergistic effect of p53 and TMZ.

Chapter 3- Materials and Methods

3.1. Materials

The pcDNA3-FLAG-p53 6.07 kbp plasmid was purchased from Addgene (Cambridge, MA, USA) and was produced and purified using a methodology developed by our research group, as outlined in the literature [192]. Tryptone and yeast extract for the bacterial cultures were obtained from Bioakar Diagnostics, while Luria-Bertani (LB) medium was acquired from PanReac. WRAP5 was synthesized using a LibertyBlue™ microwave peptide synthesizer (CEM Corporation, Matthews, NC, USA) with an additional Discover™ module (CEM Corporation, NC, USA) that combines microwave energy at 2450 MHz with the Fmoc/tert-butyl (tBu) approach. LC/MS (Waters, Saint-Quentin-en Yvelines, France) confirmed the peptide's characteristics and purity, revealing a purity of 95% or superior. WRAP5 has an NH2-LLRLLRWWWRLLRLL-CONH2 sequence with 15 residues, an isotopic mass of 2104.34 g/mol, and 5 positive charges. TMZ was acquired from Frilabo (Lisbon, Portugal), BSA, sodium dodecyl sulfate (SDS), fetal bovine serum (FBS), and Triton X-100 were purchased from Sigma Aldrich Fine Chemicals Biosciences (St Louis, MO, USA). Agarose and GreenSafe Premium were obtained from NZYTech (Lisbon, Portugal). Dulbecco's Modified Eagle's Medium (DMEM) high glucose with stable L-Glutamine was obtained from Biowest (Nuaillé, France). A Milli-Q system from Millipore (Billerica, MA, USA) was used to purify water and this ultrapure-grade water was used to prepare all the solutions. The iQuant dsDNA HS Assay kit was purchased from ABP Biosciences (Rockville, MD, USA). The human normal astrocyte cell line, HA1800, isolated from human brain (cerebral cortex) and cryopreserved, is from the American Type Culture Collection (ATCC, Manassas, USA). U-87 human cells, a cell line isolated from malignant glioma from a male patient, likely with Glioblastoma, were supplied by the European Collection of Authenticated Cell Cultures (ECACC, Salisbury, UK).

3.2. Methods

3.2.1. Bacterial growth conditions and plasmid production

The plasmid encoding for p53 was amplified intracellularly in *Escherichia coli* (*E. coli*) DH5α. Initially, *E. coli* DH5α was inoculated onto LB-agar plates containing 30 μg/mL ampicillin and incubated at 37ºC overnight. After 24 h, the isolated colonies were picked with a sterile loop and transferred to a 250 mL Erlenmeyer flask containing 62.5 mL of Terrific Broth (TB) medium composed by 20 g/L tryptone, 24 g/L yeast extract, 4 mL/L glycerol, 0.017 M KH_2PO_4 and 0.072 M K_2HPO_4 and supplemented with 30 μg/mL ampicillin. The flask was then shaken and incubated on an orbital agitator (Agitorb 200 da Aralab, Albarraque, Portugal) at 250 rpm and 37 ºC. To monitor growth, the optical density (OD) of the culture was monitored until it reached approximately 2.6, indicating the intermediate phase of bacterial growth. Once this OD was reached, a corresponding volume of the pre-fermentation culture was transferred to two 500 mL Erlenmeyer flasks, each containing 125 mL of fresh TB medium. The new flasks were incubated

and shaken at 37ºC and 250 rpm on an orbital shaker. The culture was allowed to grow for 16-18 h, until the OD at 600 nm reached approximately 9, indicating the late logarithmic phase. Fermentation was then stopped, and the culture transferred to 50 mL Falcon tubes, which were centrifuged at 1000 g for 4 min to sediment the cells. The supernatant was discarded, and the pellets stored at -20ºC. The entire process involving the cultivation of live bacteria was carried out under sterile conditions to avoid contamination.

3.2.2. Plasmid extraction and purification

After production, the plasmid was recovered using the alkaline lysis method. Initially, the bacterial pellet was resuspended in 10 mL of P1 buffer (50 mM Tris-HCl at pH 8.0, 10 mM hydrated EDTA and 100 µg/mL RNase A), followed by the addition of 10 mL of P2 buffer (200 mM NaOH and 1% SDS (w/v)). Cell lysis was promoted by gently inverting the tubes and incubating them at room temperature for 5 min. To stop the lysis, 10 mL of P3 buffer (3.0 M potassium acetate at pH 5.0 and 1% SDS (w/v)) was added, followed by incubation on ice for 20 min. The tubes were then centrifuged for 30 min at 20,000 g and 4 ºC, and the supernatant was transferred to new tubes, which were centrifuged again under the same conditions for 20 min. The anion exchange resin columns were regenerated with a solution of 0.15% Triton X-100 and 3 M NaCl, and equilibrated with QBT buffer (0.75 M NaCl, 50 mM MOPS, 15% isopropanol (v/v), 0.15% Triton X-100 (v/v) at pH 7.0). The supernatants were applied to the columns, and the proteins and low molecular weight molecules were eliminated using a low salt concentration buffer (0.5 M NaCl). Plasmid DNA was eluted directly into empty centrifuge tubes using a buffer with a higher salt concentration (1.25 M NaCl). To precipitate the pDNA, 0.7 volumes of isopropanol were added, followed by incubation on ice for 20 min. The samples were then centrifuged at 16,000 g and 4 ºC for 10 min, and the resulting pellet was resuspended in 1 mL of Tris base (10 mM, pH 8.0) and stored at -80 ºC. The 260/280 nm absorbance ratio of the samples was greater than 1.8. The conformation of the plasmid and possible contaminations were assessed by electrophoresis on a 1% agarose gel, using Tris-acetate-EDTA (TAE) running buffer (40 mM Tris base, 20 mM acetic acid and 1 mM EDTA, pH 8.0) and GreenSafe as a dye, for 30 min at 120 V.

3.2.3. Preparation of TMZ-Loaded Peptides

The preparation of TMZ-peptide mixture (TMZ-WRAP5) was carried out following a previously established protocol [192]. In summary, a solution of TMZ was prepared in ethanol at room temperature at a concentration of 0.5 mg/mL. Simultaneously, a 2 mg/mL solution of the WRAP5 peptide was prepared. Afterwards, 150 µL of the peptide solution was mixed with 360 µL of the TMZ solution in 8 mL of water in a 15 mL falcon tube. An ultrasonic bath was used to disperse the solution for 90 s. The sample was frozen overnight at -80ºC and then lyophilized for 24 h. After lyophilization, the sample was dissolved in 200 µL of ultrapure water and the peptide was quantified at 280 nm using a NanoPhotometer™ (Implen, Inc., Westlake Village, CA, USA).

3.2.4. Formation of Peptide/pDNA Complexes

To form the TMZ-WRAP5/p53 complexes, 50 µL of TMZ-peptide solutions at the required concentration according to N/P ratio were added to 150 µL of pDNA solution (1 µg dissolved in Milli-Q water) drop by drop for 1 min under vortex agitation (Figure 11). The ratio N/P is defined as the molar ratio between the positively charged amine groups (N) of the peptide and the negatively charged phosphate groups (P) of the pDNA. After the formulation, the complexes were left to equilibrate at room temperature for 25 min. The nanoparticles were then centrifuged for 20 min at 13500 x g at 4°C. The obtained pellet was stored at 4°C, up to two days, before use.

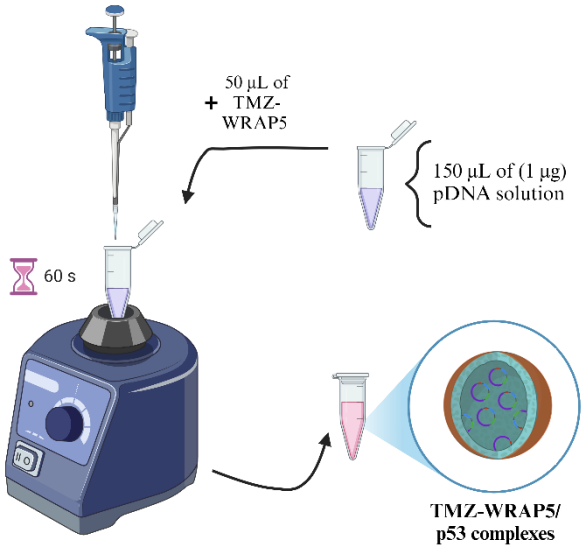

Figure 11. Schematic representation of TMZ-WRAP5/p53 complexes formation using the co-precipitation technique (drop by drop for 1 min under vortex agitation).

3.2.5. BSA coating

A 20 mg/mL solution of BSA was prepared in ultrapure water and filtered to eliminate any potential impurities or large aggregates. The BSA concentration was quantified in the NanoPhotometer™ by measuring the absorbance of the supernatant at 280 nm and the Beer-Lambert law, considering the molar extinction coefficient of 43.824 M-1 cm-1. Using this BSA solution, were prepared diluted solutions ranging from 0.08 mg/mL to 0.28 mg/mL. BSA was incorporated into the complexes by two different procedures: a) 37 µL of BSA solution was added before the complex formulation alongside the pDNA solution, here considered 0 min, and b) 25 min after the complex was formulated (and before centrifugation).

3.2.5.1. Determination of BSA coating efficiency

To quantify the protein concentration, the Pierce BCA Protein Assay Kit (Thermo Scientific, REF 23225) was used, following the manufacturer's protocol. First, a standard curve was made using BSA standards. The standards were prepared by diluting the stock solution in various

concentrations, ranging from 20 to 2,000 µg/mL with MiliQ water. The BCA working reagent (WR) was prepared by mixing 50 parts BCA reagent A with 1 part BCA reagent B (50:1 ratio). 25 µL of each standard was pipetted into a 96-well microplate. Subsequently, 200 µL of the BCA working reagent was added to each well. After mixing, the plate was covered and incubated at 37°C for 30 min. Absorbance readings were taken at an wavelength of 562 nm in the Benchmark Microplate Reader (BioRad, Vienna, Austria). The absorbance values of the BSA standards were used to generate the standard curve, which was then applied to determine the protein concentrations of the unknown samples based on their absorbance values.

After generating the BSA calibration curve (Figure 12), the protein concentration of the samples was determined, using the same protocol. For each sample, 25 µL was pipetted into the wells of a 96-well microplate. As with the standards, 200 µL of WR, mixed in a 50:1 ratio of reagent A to reagent B, was added to each well containing the samples. The plate was gently shaken and then covered and incubated at 37°C for 30 min. Following incubation, the plate was read at 562 nm using a Benchmark Microplate Reader (BioRad, Vienna, Austria).

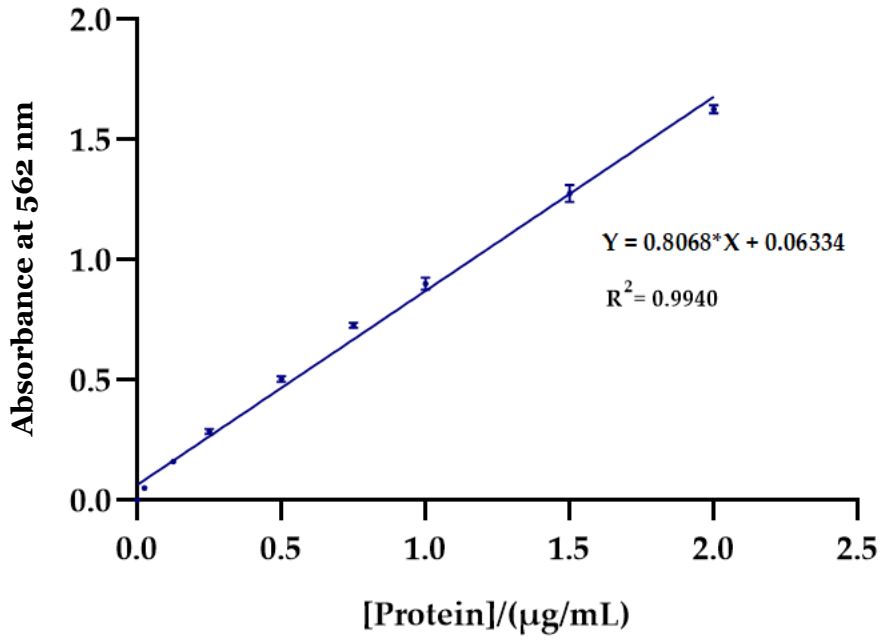

Figure 12. BSA standard curve (25-2000 µg/mL).

3.2.6. TMZ quantification

After formulation and coating with BSA as previously described, the encapsulation of TMZ in the peptides was determined. This was done using an Agilent 1260 HPLC system (Agilent, Santa Clara, CA, USA) equipped with an autosampler and a quaternary pump coupled to an Agilent 1260 Infinity VL Diode Array Detector (DAD) (Agilent, Santa Clara, CA, USA) which allows the detection of multiple wavelengths with complete spectra at sampling rates of up to 240 Hz. A

mixture of water and methanol (80:20 v/v) with 0.5 M acetic acid was used for the mobile phase, which was then subjected to vacuum filtration. The analysis was carried out using a Hypersil™ BDS C18 column (250 × 4.6 mm × 5 µM) set at 35 °C. The flow rate was set at 1.0 mL/min, and an injection volume of 20 µL was used, with a detection wavelength of 330 nm. To analyze the samples, a calibration curve (Figure 13) was first made with standard samples from 0.1 to 40 µg/mL using a TMZ stock solution concentrated at 1mg/ml. TMZ encapsulation was calculated by analyzing the peak areas of the supernatant chromatograms and the efficacy was determined using the following equation described in the literature [192] :

Drug loaded efficiency (% w/w) = (Actual drug content/Initial drug content) × 100 (1)

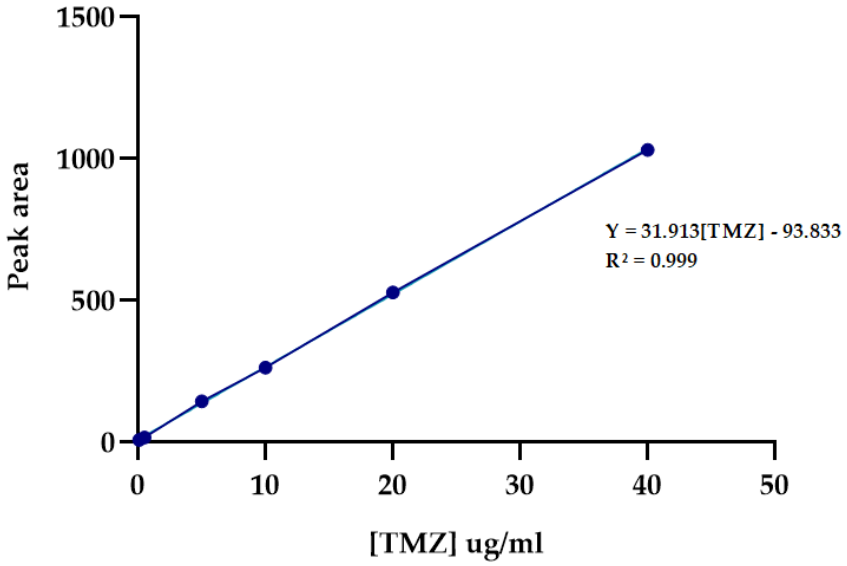

Figure 13. Calibration curve of TMZ (reference standard) obtained by HPLC method.

3.2.6. Agarose Gel Electrophoresis

The presence of pDNA in the supernatant was evaluated through electrophoresis for 40 min under 120 V in 1% (w/v) agarose gel, prepared in 50 mL 1× TAE buffer (40 mM Tris base, 20 mM acetic acid, 1 mM EDTA at pH 8.0) and stained with GreenSafe (0.6 µL). The gels were visualized using Uvitec Fire-Reader system (Uvitec Limited, Cambridge, UK).

3.2.7. Design of experiments

DoE was used to optimize the formulation of BSA-coated TMZ-WRAP5/p53 complexes with the aim of minimizing the size of the complexes, maximizing the zeta potential, maximizing the pDNA CC, and maintaining an adequate PdI- less than 0.4 (outputs). Three factors were considered as inputs, 2 numeric (namely the N/P ratio and the BSA concentration), and 1 categoric (BSA incorporation time). These inputs were studied at three levels (−1; 0; +1) and the range was defined according to preliminary studies. A central composite design (CCD) was applied,

generating 22 experiments, considering 3 replicas of a central point. Statistical analysis was performed, using Design-Expert version 11. The generalized second-order polynomial model equation used in the response surface analysis is presented below (Equation (2)):

$$Y = \beta 0 + \beta 1X1 + \beta 2X2 + \beta 3X3 + \beta 12\, X1X2 + \beta 13\, X1X3 + \beta 23\, X2X3 + \beta 11X12 + \beta 22X22 \quad (2)$$

After analyzing the suitability of the model applied to the DoE, the optimal point was determined and validated. *In vitro* studies were conducted using the conditions of the optimal point.

3.2.7.1. Particle size and zeta potential measurements

Electrophoretic light scattering and dynamic light scattering at 25°C were used, to determine complexes zeta potential, average size, and PdI. The measurements were carried out using the Zetasizer Nano ZS device (Malvern Instruments, Malvern, UK). For this purpose, the pellet was resuspended in 5% glucose with 1 mM NaCl solution and placed in a disposable universal capillary cell. The size of the complexes was determined using a He-Ne laser at 633 nm with non-invasive backscattering (NIBS). The electrophoretic light scattering mode was used to evaluate the surface charge of the nanoparticles using an M3-PALS (Phase Analysis Light Scattering) laser. The software Malvern Zetasizer v6.34 (Malvern Instruments, Malvern, UK) was used to obtain and process the data.

3.2.7.2. pDNA complexation capacity

The pDNA CC of the nanocomplexes was evaluated using the iQuant™ dsDNA HS Assay Kit. The iQuant™ working solution was prepared by diluting the iQuant™ dsDNA HS reagent in a ratio of 1:200 in 1X iQuant™ dsDNA HS Buffer immediately before use. The prepared iQuant™ working solution was then added (190 µL) to each well of a black 96-well clear bottom microplate (Greiner, Austria) to minimize fluorescence bleed-through. For the calibration curve, a series of standard dilutions of dsDNA were prepared. Subsequently, 10 µL of each dsDNA standard dilution and the supernatant of the nanoparticle samples in triplicate were added to the wells and mixed thoroughly by pipetting up and down. The microplate was then incubated at room temperature for 2 min in the dark. Fluorescence was measured using a fluorescence plate reader (SpectraMAX Microplate Reader, Molecular Devices, San Jose, CA, USA) considering an excitation wavelength of 485 nm and emission wavelength of 530 nm.

3.2.8. Scanning electron microscopy

The morphology of the BSA-coated TMZ-WRAP5/p53 complexes was evaluated by Scanning Electron Microscopy (SEM). After formation, the complexes were centrifuged, and the resulting pellet was suspended in an aqueous solution containing 40 µL of 2% tungsten. This solution was then placed on a round coverslip and left to dry overnight at room temperature. Subsequently, the samples were coated with gold using an Emitech K550 spray coater (London, England). The complexes were then visualized using a Hitachi S-2700 scanning electron microscope (Tokyo, Japan), operating at an accelerating voltage of 20 kV at various magnifications.

3.2.9. Stability in media

We studied the stability of optimal BSA-coated TMZ-WRAP5/p53 complexes after exposure to cell culture media with or without FBS supplementation. The aim was to replicate *in vitro* cell transfection conditions and simulate the extracellular environment of the human body. To conduct the test, nanocomplexes were centrifuged and suspended in 25 µL DMEM high glucose with stable glutamine, with and without supplementation with 10% FBS and streptomycin (1%)/penicillin (0.1%) antibiotics mixture solution, at 37°C. BSA-coated TMZ-WRAP5/p53 complexes were then incubated at 37°C for 4 h and the release and degradation of pDNA were monitored using 1% agarose gel electrophoresis. A pDNA sample from stock solution (non-treated with serum or FBS) and naked pDNA (non-encapsulated) incubated with 25 µL DMEM high glucose with stable glutamine at 37°C for 4 h were considered as controls. In parallel samples, 1.5 µL of 10% SDS was added and incubated for 10 min to promote the decomplexation of pDNA from the developed complexes. Samples were analyzed by electrophoresis for 30 min under 120 V.

3.2.10. Cell culture

Human astrocyte cell line HA1800 and glioblastoma cell line (U87) were cultured in 75 cm^2 T-flasks with DMEM high glucose medium supplemented with stable L-glutamine (pH 7.45), 0.5 g/L sodium bicarbonate, 10% heat-inactivated fetal bovine serum (FBS), 1.10 g/L HEPES, and 1% (v/v) penicillin-streptomycin mixture (100 µg/mL each). Cultures were maintained at 37°C in a humidified atmosphere with 5% CO2 until reaching confluence.

3.2.11. Cell Transfection

Initially, 1×10^5 U-87 cells were seeded per well in 12-well plates and cultured for 24 h in 1.5 mL of complete DMEM medium. After this period, medium was replaced with an FBS and antibiotics medium free to optimize transfection. 12 h later, complexes were added so that each well contained 1 µg of pDNA and cells were left to incubate with complexes for 4 h. After 4 h incubation, the medium was replaced with complete DMEM medium again to stop transfection process.

3.2.12. Biocompatibility test

The potential cytotoxic effects displayed by the optimal BSA-coated TMZ-WRAP5/p53 complexes were monitored in HA1800 and U-87 cells using the colorimetric MTT (3-[4,5-dimethylthiazol-2-yl]-2,5-diphenyltetrazolium bromide) assay. First, $1x10^4$ U-87 or HA1800 cells per well were seeded in 96-well culture plates and maintained at 37°C and 5% CO2. BSA-coated TMZ-WRAP5/p53 complexes were added to serum-free DMEM medium (200 µL) and applied to the wells (0.1 µg of pDNA per well) for 4 h. After transfection, the culture medium was replaced with a serum-containing medium. After 24, 48 and 72 h of incubation with the complexes, cellular viability was assessed by reducing the MTT. For this, 20 µL of MTT solution with a concentration of 2 mg/mL was added to each well for 2 h. After that, the medium was removed and 200 µL of DMSO was added to each well for 30 min with shaking to promote the dissolution of formazan crystals. The absorbance was measured using a Benchmark Microplate Reader (BioRad, Vienna,

Austria) at 570 nm. The medium without cells was set as zero absorbance and used for spectrophotometer calibration. Non-transfected and ethanol-treated cells were considered the positive and negative controls, respectively. In addition, cells transfected with TMZ and naked pDNA served as additional controls. The cellular viability was calculated using the following equation:

Cellular viability (%) = [A]test/[A]control X 100 (3)

where [A]test is the absorbance of the test sample and [A]control is the absorbance of the positive control sample.

3.2.13. Hemolysis test

To test the hemocompatibility of the optimal complexes, 2 mL of rat blood was collected in a heparinized tube supplemented with EDTA disodium salt. Subsequently, to separate the red blood cells (RBCs) the tube underwent centrifugation at 3000 rpm for 15 min at 4°C. After centrifugation, the supernatant was discarded, and the RBCs were washed with a 0.85% w/v saline (NaCl) solution until clearness of the supernatant was achieved. Upon the washing process, a suspension of RBCs at a concentration of 3-5% was prepared in phosphate-buffered saline (PBS) pH of 7.4. 900 µL of this RBC suspension was further incubated with 100 µL of the optimal BSA-coated TMZ-WRAP5/p53 complexes each one resuspended in PBS pH of 7.4, for 1 h at 37°C. For comparative analysis, PBS at pH 7.4 and Triton X-100 (1% solution) were employed as negative and positive controls, respectively. Upon conclusion of the incubation period, samples were centrifuged at 8000 rpm for 20 min. The absorbance of the supernatant was measured at 576 nm utilizing a UV-visible spectrophotometer (BioRad, Vienna, Austria), and the percentage of hemolysis was calculated considering the equation:

Hemolysis (%) = (Abs. Sample – Abs. Negative control) / (Abs. Positive control – Abs. Negative control) x 100 (4)

3.2.14. Gene transcription

3.2.14.1. RNA extraction

24 h after transfection, cells were collected for total RNA extraction. Firstly, culture medium was removed from wells, and cells were washed three times with phosphate-buffered saline (PBS). Next, 300 µL of TripleXtractor (GRiSP, Porto, Portugal) was added and incubated at room temperature for 5 min. After incubation, the cell suspension was transferred to Eppendorf tubes, where 60 µL of chloroform is added. The mixture is vortexed for 15 s to separate the different biomolecules within the sample and incubated for a further 15 min at room temperature. The samples are then centrifuged at 12,000 g and 4 °C for 15 min. The upper phase, containing the RNA, is carefully transferred to new Eppendorf tubes, to which 150 µL of isopropanol is added to precipitate the RNA. The samples are incubated and centrifuged again under the same conditions. The pellet formed is resuspended in 75% ethanol (prepared in diethylpyrocarbonate (DEPC)

water) to remove the organic compounds, followed by centrifugation for 5 min at 12,000 g and 4 ºC. The supernatant was removed, and the pellet was air-dried and resuspended in 20 µL of nuclease-free water and quantified using a NanoPhotometer™. Additionally, the RNA was analyzed by 1% agarose gel electrophoresis.

3.2.14.2. cDNA synthesis

The cDNA synthesis was made using Xpert cDNA Synthesis kit (GRiSP Research Solutions, Porto), following the manufacturer's protocol. In a RNase free tube was added 4 µL of Reaction Buffer, 1 µL of dNTP's, 1 µL of Random primer, 1 µg of Template RNA and RNase free water to make a total volume of 13 µL. The samples were processed in a thermal cycler with an initial incubation at 25ºC. For qPCR, the samples were incubated at 50ºC for 15 min, while for PCR, they were incubated at 50ºC for 50 min. Subsequently, the reverse transcriptase enzyme was inactivated by heating at 85ºC for 5 min, followed by cooling at 4ºC for 2 min. Finally, the samples were stored at -20ºC for preservation until further analysis.

3.2.14.3. Conventional polymerase chain reaction (PCR)

The p53 cDNA was amplified by conventional PCR method using the Speedy Supreme NZYTaq 2× Green Master Mix (NZYTech, Lisbon, Portugal), following the manufacturer's protocol. The amplification reaction was prepared by mixing the necessary components in a 50 µL reaction volume. This included 25 µL of Speedy Supreme NZYTaq, 2 × Green Master Mix, 1 µL of primer reverse (5′-CTG AGT CAG GCC CTT CTG TCTT-3′), and primer forward (5′–GAG CTG AAT GAG GCC TTG GA-3′) diluted in 1:20, 1 ng of cDNA and nuclease-free water to prefill the final volume.

The PCR program was set up in a T100™ Thermal Cycler (Bio-Rad Laboratories, Inc., Hercules, CA, USA), starting with an initial denaturation step at 95 °C for 5 min to ensure the DNA strands were fully denatured. This was followed by 30 cycles of amplification. Each cycle included denaturation at 94 °C for 2 s, annealing at 55 ºC for 5 s, and extension at 72 °C 5 s. A final extension at 72 °C for 2 min after which the samples were held at 4 °C. PCR products were analyzed by electrophoresis on an 1 % agarose gel and visualized in the Uvitec Fire-Reader system.

3.2.14.4. qPCR

The p53 cDNA was amplified by qPCR method using NZY Supreme qPCR 2x Green Master Mix (NZYTech, Lisbon, Portugal), following the manufacturer's protocol. The qPCR reactions were prepared in a total volume of 20 µL, containing 10 µL of the 2× Master Mix, 1,6 µL of primer reverse (5′-CTG AGT CAG GCC CTT CTG TCTT-3′), and primer forward (5′–GAG CTG AAT GAG GCC TTG GA-3′) diluted in 1:20, 1 µL (1 ng) of cDNA and 5,8 µL of nuclease-free water to prefill the total volume. The housekeeping gene GFAP (Glial Fibrillary Acidic Protein) was used as a control to normalize the p53 expression levels.

The PCR program was set up in a T100™ Thermal Cycler (Bio-Rad Laboratories, Inc., Hercules, CA, USA), beginning with an initial denaturation at 95°C for 2 min. This was followed by 40 cycles of denaturation at 95°C for 5 s, annealing at 60°C for 30 s. After amplification, a melt curve analysis was performed by gradually heating from 55°C to 95°C, with a temperature increment of 5°C in 10 s. The relative expression of p53 was calculated by comparing the Ct (threshold cycle) values of p53 to the housekeeping gene GFAP using the ΔΔCt method.

3.2.15. Statistical Analysis

The statistical analysis involved a one-way analysis of variance (ANOVA) followed by the Bonferroni test. All quantitative data are presented as the mean ± SEM based on at least three measurements. Data analysis was performed using GraphPad Prism V9.0.0 software. A p-value below 0.05 was considered statistically significant. Additionally: ** indicates $p \leq 0.01$; *** indicates $p \leq 0.001$; **** indicates $p \leq 0.0001$.

Chapter 4- Results and discussion

4.1. Formation of BSA coated TMZ-WRAP5/p53 complex

The developed complexes are composed of a cell-penetrating peptide (WRAP5), TMZ, and plasmid DNA, leading to the formation of nanoparticles by co-precipitation induced by the electrostatic interactions between the positively charged amine groups of the peptide and the negative phosphate groups of pDNA. In the process, these complexes entrap and/or adsorb TMZ. The BSA was added to the TMZ-WRAP5/p53 complexes at two different times, 25 min post formulation and before formulation - at 0 min (Figure 14). These two different procedures were studied to unravel the influence of BSA into complexes formation and in order to optimize the BSA coating process. BSA can bind to peptides at the complexes through various molecular interactions. The BSA hydrophobic regions facilitate the binding to the hydrophobic areas of the peptide. In addition, due to its negative charge, albumin can form ionic bonds with WRAP5 peptide, which has a positive charge of +5, or positively charged complexes [193].

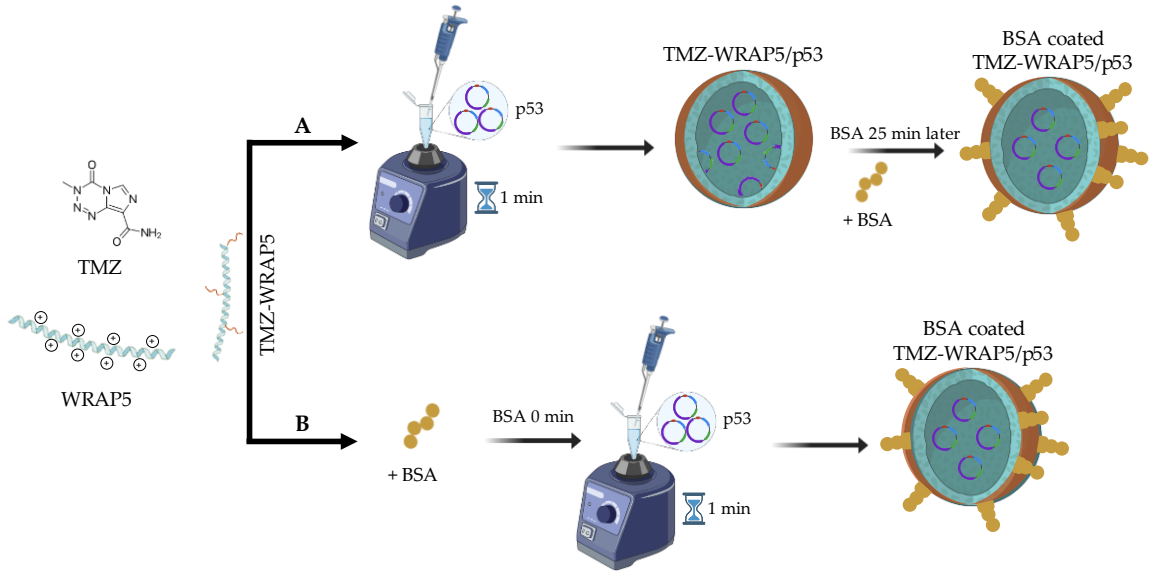

Figure 14. Illustrative scheme showing the formation of the complexes. A) BSA-coating 25 min after formulating the TMZ-WRAP5/p53 complexes; B) BSA coating before formulating the TMZ-WRAP5/p53 complexes, considered 0 min.

Albumin-based complexes have been widely used due to their beneficial properties, such as biodegradability, lack of antigenicity, and surface modification to mitigate adverse drug toxicity [194]. In addition, albumin-based nanoparticles can break through the BBB and selectively target tumor cells through different mechanisms [195]. Tumor cells within glioma tissues exhibit heightened albumin uptake, relying on it as a vital amino acid and energy source [196]. To bolster albumin absorption within gliomas, there is an upregulation of secreted protein acidic and rich in cysteine, SPARC- an albumin-binding protein. Given the SPARC glioma cells overexpression, coating the complexes with albumin can be expected to improve tumor targeting, and enhance

specificity within this system [174, 196]. This molecule has been extensively explored in the treatment of cancer with different types of nanoparticles, from iron oxide magnetic nanoparticles where the BSA-coated magnetic nanoparticles were prepared as curcumin (CUR) carriers through desolvation and chemical co-precipitation process for breast cancer treatment [197] or gold nanoparticles coated with BSA for cancer photothermal therapy [198].

TMZ-WRAP5/p53-based complexes have already been revealed to possess adequate characteristics that merit further study in the context of glioblastoma therapy [192]. In this work, we explored the BSA-coating of these TMZ-WRAP5/p53 nanocomplexes to enhance their non-immunogenic profile and lyoprotection, as the coating can function as stable shells. The optimization of the formulation process of BSA-coated TMZ-WRAP5/p53 complexes can, therefore, enhance their physico-chemical properties which will contribute to their targeted and co-delivery performance toward glioblastoma.

4.2. BSA encapsulation efficiency

The protein concentration of the complexes was quantified using the *Pierce BCA Protein Assay Kit*, strictly following the protocol recommended by the manufacturer. The standard curve was constructed from serial dilutions of BSA. The BSA standard curve, constructed with the obtained absorbance values, proved to be linear at the analyzed concentrations, allowing precise quantification of the proteins in the samples. The protein concentration results for the complexes revealed that the BSA-coated TMZ-WRAP5/p53 complex achieved a concentration of 9.856 µM, corresponding to 81.32% of the BSA added to the complex during formulation. This high percentage highlights the efficiency of BSA incorporation into the complex. Successful coating with BSA is a critical aspect of this work, as it plays a key role in enhancing the stability, biocompatibility, and functional delivery of the complex, thereby contributing to the overall effectiveness of the formulation.

4.3. TMZ encapsulation

To obtain an accurate quantification of TMZ in the peptide complexes, a high-performance liquid chromatography with diode array detection (HPLC-DAD) method was used. The calibration curve was generated by plotting the ratio of the analyte's peak area to its concentration. Each calibration point represents the mean value (Mn) ± standard deviation (SD) of triplicate measurements, producing a correlation coefficient (r^2) above 0.99, confirming the accuracy and linearity of the method. The analysis revealed that the peptide did not interact with the C18 column under the applied isocratic conditions, since no peptide peaks were detected. This lack of interaction confirms that TMZ can be detected accurately without interference from the peptide.

Using this method, the TMZ encapsulation efficiency was determined to be 66.9%, calculated by comparing the initial amount of TMZ with the amount retained in the peptide solution. This high

level of encapsulation efficiency highlights the successful incorporation of TMZ into the peptide complex, which is crucial.

4.4. DoE parameters

In recent years, nanotechnology has emerged as a promising avenue for cancer therapy, mainly due to the ability of nanoparticles to serve as genetic and pharmacological vehicles[199, 200]. It offers a range of benefits, such as enhancing existing therapies with superior targeting capabilities, boosting the effectiveness of localized drugs, and reducing systemic toxicity among other assets [201]. Given the unique environment of tumors and their vascularization, nanosystems require specific characteristics. In general, ideal features of nanoparticles include a size ranging from 100 to 200 nm and a positive surface charge to promote cell internalization[174]. Furthermore, in the field of gene therapy, obtaining a high gene encapsulation rate is crucial for an effective therapeutic response. In this sense, it is clear that the rational design and optimization of the nanosystem properties are crucial steps to achieve high delivery and therapeutic performance.

DoE is a systematic method used in research and industrial processes to determine the relationship between factors affecting a process and the output of that process. DoE contributes to the planning, conduction, analysis, and interpretation of controlled tests to evaluate the factors that may influence a particular outcome or set of outcomes. The DoE application was considered to optimize the properties of BSA-coated TMZ-WRAP5/pDNA complexes for the simultaneous delivery of TMZ and TP53 gene for glioblastoma therapy. By exploring DoE tools, the main aim was to unravel how input/factors (alone and/or combined) affect the formulation properties (responses)[182]. Based on previous results conducted by our research group, which showed the ability of these complexes to form at low N/P ratio [45], here a range between N/P 0.5 and 1.5 was defined as input in the DoE.

Concerning the BSA coating of the peptide complexes, initial analyses were carried out to establish a suitable range for the BSA. Complexes were prepared by adding BSA either before or 25 min after formulation, in concentrations ranging from 0.05% to 0.5%. The supernatants were analyzed using agarose gel electrophoresis to evaluate the pDNA CC. The results presented in the Figure 15, indicated that when BSA concentration exceeded 0.3%, the complexes were unable to fully incorporate the pDNA, resulting in concentrations ranging from 12.12 μM (0.08%) to 42.42 μM (0.28%), with the BSA-coating before complexes formulation (at 0 min) or 25 min after formulation. Preliminary studies demonstrated that both N/P ratio and BSA concentration, as well as the timing for the BSA-coating process, are variables influencing the properties of TMZ-WRAP5/p53 nanocomplexes. Therefore, these parameters were taken as the inputs of DoE. The

size, polydispersity index, surface charge, and pDNA CC were the selected properties as DoE outputs.

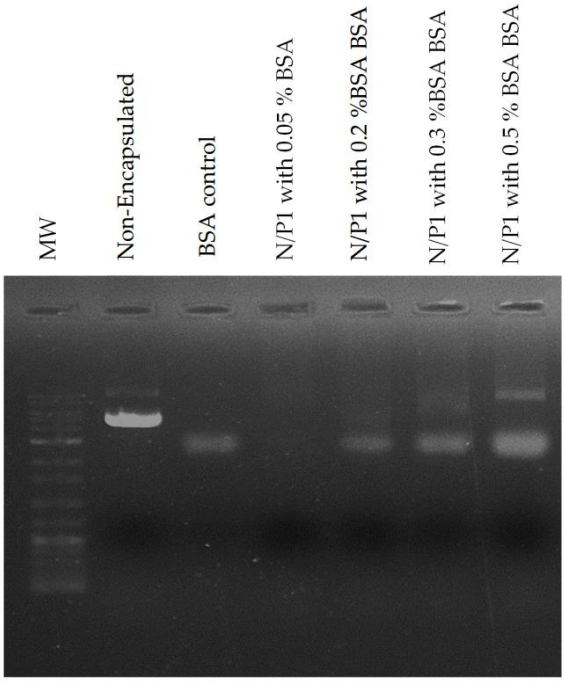

Figure 15. Electrophoretic analysis of BSA-coated TMZ-WRAP5/pDNA complexes at an N/P ratio of 1 and BSA concentration ranging from 0.05% to 0.5%. Lane 1: DNA Molecular Weight Marker; Lane 2: non-encapsulated pDNA (control); Lane 3: BSA control sample.

4.5. DoE application: finding the optimal formulation

After establishing the inputs for the DoE, a CCD was implemented to optimize the formulation of TMZ-WRAP5/p53 complexes. This particular model is suitable for this work because does not take into account points outside the range established for the inputs, which we already know for the preliminary studies that can lead to negative results due to the aggregation of nanoparticles [202]. Central composite models aim to estimate the non-linearity of response data and determine the curvature of continuous responses. They also make it easier to reduce the number of tests needed to estimate the squared terms in second-order models. In this way, central composite models have great value in experimental design and analysis [203, 204].

Table 1 gives a comprehensive overview of all the runs suggested by the DoE, separated by BSA addition time – 0 min or 25 min - (categoric input), with both N/P ratio and BSA concentration parameters listed in ascending order. To assess the reproducibility of the model, three central points (n = 3) were run under identical conditions, highlighted in grey in Table 1 the Design Expert software designed 22 experiments and the respective outputs zeta potential, size, and PdI were revealed by electrophoretic and dynamic light scattering and using the dsDNA HS Assay Kit was determined the pDNA CC (%).

Table 1. Composite central design and outputs for the considered inputs.

Inputs	Outputs					
Time (min)	N/P Ratio	BSA (%)	Charge (mV)	Size (nm)	PdI	pDNA CC (%)
0	0.5	0.08	-17.3	359.20	0.580	35.5
	0.5	0.18	-17.7	358.00	0.490	26.8
	0.5	0.28	-31.6	431.84	0.483	25.8
	1.0	0.08	3.8	250.82	0.378	86.4
	1.0	0.18	-1.0	307.67	0.361	80.3
	1.0	0.18	0.9	299.44	0.344	78.3
	1.0	0.18	1.2	290.97	0.381	76.7
	1.0	0.28	-3.4	308.2	0.480	86.9
	1.5	0.08	1.9	217.94	0.370	91.0
	1.5	0.18	2.6	243.96	0.310	89.0
	1.5	0.28	1.1	280.60	0.331	91.7
25	0.5	0.08	-12.4	311.25	0.391	51.2
	0.5	0.18	-18.3	324.99	0.309	39.4
	0.5	0.28	-25.7	350.13	0.276	27.0
	1.0	0.08	9.0	182.84	0.281	97.1
	1.0	0.18	5.0	211.47	0.214	91.4
	1.0	0.18	3.2	203.47	0.242	90.9
	1.0	0.18	4.5	207.74	0.234	87.2
	1.0	0.28	0.0	218.90	0.290	91.8
	1.5	0.08	11.6	134.09	0.223	95.3
	1.5	0.18	8.6	175.37	0.224	91.7
	1.5	0.28	1.3	193.59	0.228	95.8

At BSA addition time zero, with the increase of BSA percentage in the formulation, we observed an increase in the size of the complexes, but a decrease in complexes surface charge and, for most conditions, a decrease in pDNA CC. It was observed that increasing the concentration of BSA significantly increases the size of the complex. This fact can contribute to the higher size of the BSA molecule (7.1 nm and a molecular mass of 66.5 kDa) compared to the size exhibited by pDNA. This trend between the complex size and the BSA concentration has been previously documented [205]. Regarding the pDNA CC, the decrease in this parameter with BSA concentration may be due to the competition of electrostatic interactions with the peptide between BSA and pDNA [206, 207]. Adding BSA at time 0 of the formulation can decrease the ability of the peptide to complex with the pDNA [208]. This phenomenon also leads to a more negative surface charge since BSA is negatively charged at physiological pH [209-212]. For instance, at an N/P ratio of 0.5, the nanoparticle size increases from 359.2 nm at 0.08% BSA to 431.84 nm at 0.28% BSA. Concurrently, the zeta potential becomes more negative, shifting from -17.3 mV to -31.6 mV. Similarly, at an N/P ratio of 1.0, higher BSA concentrations lead to an increase in nanoparticle size from 250.82 nm to 308.2 nm and a shift in zeta potential from a positive +3.8 mV to a negative -3.4 mV. The amount of BSA added to the complexes did not significantly alter the PdI, showing some uniformity among these conditions. These findings support the idea that BSA

concentration can affect the characteristics displayed by complexes. The N/P ratio also influenced the properties of the complexes, but in an opposite way when compared to the effect of BSA. Naturally, by increasing the N/P ratio, the charge of the complexes increases, becoming more positive, and the size decreases. At higher ratios, a greater amine content is present in the formulation, which strengthens the interaction between peptide and pDNA leading to an increase in pDNA condensation. These conditions favor smaller complexes, more positive charges at the complex surface, and higher pDNA CCs [192]. We can see this behavior on the lowest N/P ratio (0.5) displaying sizes greater than 300 nm, specifically, 359.2 nm at 0.08% BSA and 431.84 nm at 0.28% BSA, compared to sizes below 300 nm for higher N/P ratios, such as 250.82 nm at an N/P ratio of 1.0 and 0.08% BSA. The PdI was also lower for high N/P ratios. The pDNA CC also reduces significantly when the ratio decreases, leading to significant differences within each addition time ranging from 35% (N/P 0.5) to 91% (N/P 1.5) at 0 min. This tendency of lower pDNA CCs at low N/P ratios was also found in a previous study by our research group, in which TMZ-WRAP5/pDNA complexes were formulated at different N/P ratios (0.1, 0.5, and 1) [192].

When BSA was added 25 min after formulation, the trend remained the same; increasing BSA concentration generally led to more negatively charged particles, larger sizes, and a less efficient pDNA CC. Higher N/P ratios yielded more positively charged particles, with smaller size and higher pDNA CC values. As presented in Table 1, at an N/P ratio of 0.5, increasing the BSA concentration from 0.08% to 0.28% leads to a size increase from 311.25 nm to 350.13 nm, and the surface charge became more negative, changing from -12.4 mV to -25.7 mV. The pDNA CC also decreased significantly from 51.2% to 27%. At a BSA concentration of 0.08%, increasing the N/P ratio from 0.5 to 1.5 resulted in a significant decrease in particle size from 311.25 nm to 134.09 nm. The surface charge also shifted from -12.4 mV to 11.6 mV, and the pDNA CC improved dramatically from 51.2% to 95.3%. These phenomena are in line with the bibliographical information mentioned for time 0 [45].

The time of BSA addition proved to be a relevant input, generally altering the outputs. The complexes coated with BSA 25 min after formulation showed more favorable properties for payload intracellular delivery, such as more positive surface charges, decreased sizes, and lower PdI. At an N/P ratio of 1.0 and 0.18% BSA, the complexes size decreased from 299.5 nm at 0 min to 203.5 nm at 25 min, the zeta potential increased from + 0.9 mV to + 3.2 mV, and the pDNA CC improved from 78.3% at 0 min to 91.0% at 25 min. These complexes also generally displayed a lower PdI, such as decreasing from 0.344 at 0 min to 0.242 at 25 min, which reveals the uniformity in the particle size distribution. The main output indicating significant improvement with BSA coating at 25 min compared to the one at 0 min is the pDNA CC. This enhancement is corroborated by electrophoresis gel analysis of the supernatants of the BSA-coated TMZ-WRAP5/pDNA complexes. The electrophoresis study demonstrates that by performing BSA addition at 0 min, the pDNA condensation is lower, as evidenced by the presence of pDNA in the supernatant. In contrast, by adding BSA 25 min after complexes formulation, pDNA is observed in the supernatant only for samples with lower N/P ratios, indicating improved pDNA CC.

Considering the goal of achieving BSA-coated TMZ-WRAP5/p53 complexes with higher surface charge, smaller size, a PdI between 0.2 and 0.3, and pDNA CC near 100%, it becomes notorious that complexes display favorable attributes when they are formulated at higher ratios (N/P 1 and N/P 1.5) and reduced quantities of BSA (0.08%-0.18%) added 25 min after formulation.

Table 2 shows the multiple regression equations, the model applied to each output, and the statistical coefficients. The equations, given by the Design Expert analysis, correlate the results with the different inputs, with indication of positive or negative effect on the results by the sign underlying each factor [202]. With this approach, we achieved a deep understanding on the relationship between the independent variables and the respective results, highlighting their direction and effect. It is possible to analyze the influence of three key factors – N/P ratio (A), BSA concentration (B), and BSA coating time (C) - on four different responses: surface charge, size, PdI and pDNA CC as presented in Table 2. In the case of surface charge, significant positive effects of N/P ratio and BSA coating time were observed, along with a negative impact of BSA concentration. Increasing the N/P ratio results in a positive effect on the complex charge, due to the greater amount of positively charged amino groups from the WRAP5 peptide [192]. On the other hand, increasing the amount of BSA increases the content of negative charges in the system, which has a negative effect on the overall charge of the BSA-coated TMZ-WRAP5/p53 complexes. These changes are evident in the variations in the size and charge of the nanoparticles outlined in the table. For example, at an N/P ratio of 0.5 and 0.28% BSA, the negative charge increases significantly to -31.6 mV, while the particle size also grows to 431.8 nm. In contrast, at an N/P ratio of 1.0 and the same concentration of BSA, the charge is less negative (-3.4 mV) and the particle size is smaller (308.2 nm).

Table 2. Multiple regression equations, the response surface model, and the statistical coefficients provided by the DoE analysis

Output	Multiple Regression Equations	Model	R2	R2 Adjusted	R2 Predicted	Adequate Precision
Charge	+ 2.88 + 12.51 A - 4.58 B + 2.10 C + 2.06 AB + 0.47 AC - 0.86 BC – 9.94 A2 - 1.39 B2	Quadratic	0.9841	0.9744	0.9317	31.863
Size	+ 248.72 - 74.15 A + 27.26 B - 37.95 C +1.33 AB - 6.40 AC - 4.85 BC + 33.97 A2 - 1.42 B2	Quadratic	0.9786	0.9654	0.9371	31.522
PdI	+ 0.30 - 0.070 A - 0.011 B - 0.073 C + 0.022 AB + 0.020 AC – 0.0056 BC + 0.019 A2 + 0.043 B2	Quadratic	0.9296	0.8863	0.7335	16.326
pDNA CC	+ 78.39 + 28.06 A - 3.13 B + 1.84 C + 4.39 AB - 1.53 AC - 1.71 BC - 20.55 A2 + 8.27 B2	Quadratic	0.8436	0.7474	0.7292	8.405

Similarly, size showed significant positive associations with both N/P ratio and BSA coating time, but a negative relationship with BSA concentration. The PdI was mainly influenced by the N/P ratio and BSA coating time, with negligible effects from BSA concentration. The pDNA CC showed positive relationships with the N/P ratio and BSA concentration, although with a lesser influence on coating time. However, it is evident that the influence of the input variables alters across the different outputs. Overall, the interaction of BSA coating time and N/P ratio always shows a positive effect on the four evaluated responses, while the interaction of the factors of N/P ratio and % BSA demonstrates a negative effect for all responses. These results of the factor interactions corroborate the influence of each independent factor and suggest that BSA coating time has a predominant positive influence.

The quadratic model was applied to all outputs. This model provides a robust framework for capturing nonlinear relationships between independent variables and the response, improving predictive capability across a broad range of input values. The quadratic model facilitates the identification of optimal experimental conditions, offering precision in achieving desired outcomes such as maximizing yield or minimizing defects [213]. The statistical coefficients obtained for each response are presented in Table 2 and were applied to unravel whether the statistical models generated from these experiments are valid and fit the data. The coefficient of determination (R^2) gives insight in how well the regression model fits the data and it should be close to 1 to evaluate if the model has high significance and the fitness of the output statistical model to the data [214]. The R^2 values for the four outputs range from 0.8436 to 0.9841, suggesting the model fits the data. These values indicate that a proportion of the variability in the results can be attributed to the independent variables included in the model. Furthermore, the adjusted R^2 values, which consider the number of predictors and penalize overfitting, remain high, ranging from 0.7474 to 0.9744. This suggests that the model explains the variability of the results, taking into account the complexity of the model [190]. The predicted R^2 values reflect the predictive accuracy of the model, ranging from 0.7292 to 0.9371, indicating moderate to high levels of predictive ability of new data. The appropriate accuracy values represent the signal-to-noise ratio, suggesting variable levels of predictability between the results, with higher values suggesting the validity of the model to navigate the design space [190].

Table 3 shows the ANOVA analysis carried out to evaluate the significance of each factor and interaction term for the results of surface charge, size, PdI, and pDNA CC. This was achieved by comparing the variability of residuals of the current model with the variability between observations and replicate configurations of the factors. The results summarized in Table 3, demonstrated the statistical significance of the model for all outcomes, as indicated by p-values of less than 0.0001 for charge, size, and PdI, and 0.0004 for pDNA CC. Factor A (N/P ratio) showed statistically significant effects on all results, with p-values of less than 0.0001. Factor B (BSA concentration) was significant only for charge and size outputs and factor C (BSA coating time) was significant for all outputs, except for pDNA CC. In the interaction terms AB, AC, and BC, only AB was significant for the charge output. The quadratic terms A^2 and B^2 exhibited mixed

significance in the outputs. In addition, p-values of lack of fit were non-significant (> 0.05) for all outputs. In conclusion, based on the results presented, the DoE model effectively fitted the data.

Table 3. Analysis of Variance (ANOVA) Results for Central Composite Design.

Source	Charge	Size	PdI	pDNA CC
Model	<0.0001	<0.0001	<0.0001	0.0004
A	<0.0001	<0.0001	<0.0001	<0.0001
B	<0.0001	<0.0001	0.2746	0.4358
C	0.0002	<0.0001	<0.0001	0.5340
AB	0.0085	0.7898	0.0884	0.3734
AC	0.3981	0.1329	0.0626	0.7003
BC	0.1383	0.2456	0.5809	0.6682
A^2	<0.0001	<0.0001	0.2275	0.0044
B^2	0.1203	0.8211	0.0137	0.1903
Lack of fit	0.0961	0.0501	0.0550	0.9982

After understanding the impact of each input on the respective output, conducting statistical analysis on the coefficients, analyzing variance, and validating the statistical models of the DoE, the Design-Expert software predicted the optimum point for the BSA-coated TMZ-WRAP5/p53 nanocomplexes to maximize the pDNA CC and the positive surface charge, and at the same time to minimize the size and PdI. Table 4 presents the N/P ratio (A=1.03), the amount of BSA (B= 0.08%), and the BSA coating addition time (C=25 min) that is required to obtain the optimal formulation of the complexes, as well as the predicted outputs and a range of values for the validation of each output (95% of confidence interval). The predicted values for charge, size, PdI, and pDNA CC are +11.15 mV, 144.3 nm, 0.238, and 97.1%, respectively. Based on these values, the optimum point selected by DoE was tested in triplicate (n=3) and the outputs were validated according to the data expected by Design-Expert software (Table 4). The optimal point revealed a zeta potential of +9.8 mV. This positive charge enhances cellular internalization, as the complexes can effectively interact with anionic-sulfated proteoglycan molecules located on the cell surface [215]. The complexes presented a size of 182.3 nm, which is a beneficial size for cellular uptake. It is assumed that delivery systems displaying a size range of 100–200 nm, by preference, internalized by cells and via endocytosis (clathrin- or caveolin-mediated processes) [216, 217]. Optimal complexes have a PdI of 0.248 that shows a high degree of uniformity in the particle size distribution within a sample [218], and a pDNA CC of 96.5% ensures efficient pDNA loading/incorporation contributing to potential high gene expression and, therefore, enhanced therapeutic effect.

.

Table 4. Optimal point prediction and obtained mean

Predicted input	output	Predicted Mean	95% CI low for mean	95% CI High for Mean	Obtained Mean
A- 1.03	Charge	9.7	7.2	12.2	9.8
B- 0.08%	Size	181.5	163.0	200.0	182.3
C- 25	PdI	0.286	0.240	0.332	0.248
	pDNA CC	94.8	76.8	112.8	96.5

After the validation of the DoE, the properties of the same complexes without BSA, which served as a control for the following studies, were analyzed. The TMZ-WRAP5/pDNA complexes had a surface charge of +13.4 mV, size of 140.7 nm, a PdI of 0.220, and a pDNA CC of 99.8%. The characteristics of the complexes without BSA coating allowed us to conclude that BSA was successfully inserted into the system. There was a slight decrease in the system's charge, due to the negative charge of the BSA, and an increase in their size. DoE was revealed to be very useful in determining the role of BSA on the properties exhibited by the BSA-coated complexes, and in determining the conditions at the formulation step that induces the conception of the "ideal" BSA-coated TMZ-WRAP5/pDNA complexes – the ones bearing the most favorable properties in terms of size, surface charge, PdI, and pDNA CC. In this sense, the DoE approach gave us control over the characteristics of the nanocomplexes formed, which may represent a great achievement in the design/development of co-delivery systems toward efficient glioblastoma therapy.

4.6. Scanning electron microscopy

SEM was used to evaluate the morphology of the optimal point and the control, and the resulting images are shown in Figure 16. The BSA-free TMZ-WRAP5/pDNA complexes (A) had a spherical shape with a visibly smooth surface. On the other hand, the BSA-coated TMZ-WRAP5/pDNA complexes (B), exhibited a different morphology characterized by a more angular and textured appearance with sectional view of a circle inside a squared or hexagonal shaped coating layer. These results suggest that the BSA coating significantly influences the morphology of the TMZ-WRAP5/pDNA complexes and proves unequivocally that the coating was effective, with the BSA being probably located on the outside of the complexes.

The observed changes in morphology suggest that the BSA coating suggests an improvement to their biological behavior. For instance, the textured coating could influence interactions with cellular membranes, enhance circulation time by evading immune recognition, or improve cellular uptake [219]. Additionally, the morphology indicates that BSA effectively coats the exterior of the complexes, likely enhancing their biocompatibility by providing a proteinaceous interface that mimics natural biological systems [219].

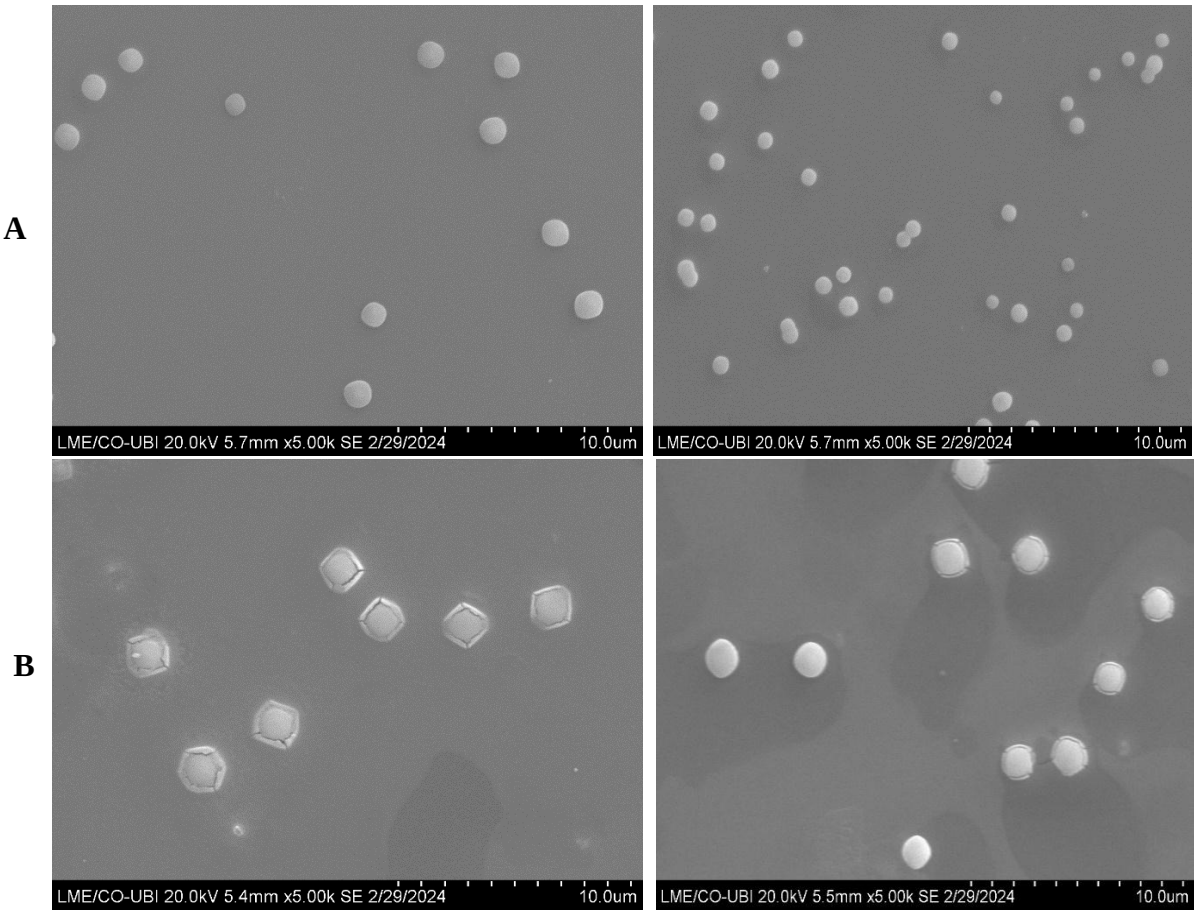

Figure 16. Scanning electron micrographs of BSA-free TMZ-WRAP5/pDNA complexes prepared at N/P ratio of 1.03 (A) and BSA coated- TMZ-WRAP5/pDNA complexes prepared at N/P ratio of 1.03 with 0.08% BSA (B). Scale bar = 5 µm

I'm aware that the obtained sizes from SEM analysis are not in full agreement with data from DLS. SEM allows for direct imaging of dry particles and an alteration in the size of the complexes during the acquisition of micrographs is expected. DLS can be interpreted as an indirect assay for size determination as it is based on the intensity of molecular movement, it measures the hydrodynamic radii of the particles, which includes the particle itself but also the ionic and solvent layers associated with it in solution under the experimental defined conditions. DLS models the size from this data. Therefore, DLS data cannot be directly compared to dimensions provided by experiments conducted with other techniques. In this work, we considered DLS more reliable. However, at this stage we must highlight that choosing a technique to characterize a nanosystem should take into consideration factors such as, the expected size and the composition of the molecules and various techniques along with accurate interpretation of data must be advantageous.

4.7. Stability in media

Evaluating the stability of BSA-coated TMZ-WRAP5/pDNA complexes in the extracellular environment and verifying the protection of the transgene are critical due to their significant impact on transfection success. To comprehensively investigate these aspects, we conducted protection and stability studies on optimal TMZ-WRAP5/pDNA complexes, both with and without BSA. The results presented in Figure 17 demonstrated the stability and integrity of pDNA during a 4 h incubation period, as indicated by the absence of any pDNA bands on the agarose gel for both BSA-coated and non-coated TMZ-WRAP5/pDNA complexes. The absence of bands in the gel indicates that the pDNA remained intact throughout the incubation process, highlighting the protective capacity of the developed complexes. In contrast, non-encapsulated pDNA (Lane 3) was completely degraded after its incubation with DMEM high glucose with stable glutamine for 4 h. The results also demonstrated that through decomplexation by SDS, the pDNA was effectively released from the complexes without any signs of degradation showing a predominant supercoiled isoform after being released (Figure 17). The supercoiled isoform of pDNA is critical for gene delivery as it is the most bioactive form and the isoform that promote higher levels of gene expression, such as for the p53 gene [220]. This further confirms the stability and protective nature of the optimal BSA-coated TMZ-WRAP5/pDNA complexes. The observed stability ensures that the pDNA remains protected from enzymatic degradation and other destabilizing factors present in the biological environment [221]. This protection is vital for maintaining the therapeutic effectiveness of the delivered genetic material.

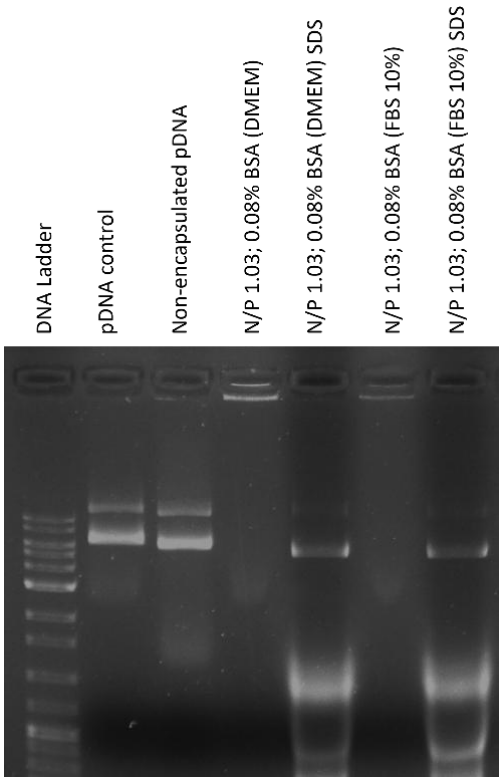

Figure 17. Electrophoretic analysis of the stability displayed by the optimal BSA-free and BSA-coated TMZ-WRAP5/p53 complexes after 4 h of incubation with DMEM high glucose with stable glutamine medium with 10% FBS or only 10% FBS. Lane 1: pDNA Molecular Weight Mark.

4.8. Biocompatibility

Cytotoxicity analysis is an important step in the evaluation of the potential utility of delivery systems for biomedical uses. The toxicity displayed by nanosystems could severely limit their effectiveness in facilitating successful drug/gene therapy. To assess the biocompatibility profile of optimal BSA-coated TMZ-WRAP5/p53 complexes an MTT assay was performed on human astrocytes at different incubation times (24, 48, and 72 h). The same experiment was performed with the correspondent BSA-free complexes to reveal the impact of BSA coating on cellular viability. The use of astrocyte cells provides insight into the specific interactions of the TMZ/p53 complexes with cells directly involved in glioblastoma disease. Also, by focusing on astrocytes we were able to mimic the microenvironment of glioblastoma tumors. The results for the performed MTT assay are displayed in Figure 18. At 24 h, the pDNA-only complexes with an N/P ratio of 1.03 showed similar viability to the control cells, 94% and 93% respectively, indicating their non-toxic profile. With the addition of 0.08% BSA, the viability of the cells was 91%, suggesting very low toxicity. In the 48 h and 72 h tests, the trend remained consistent. At 48 h comparisons between the control cells and the complexes with an N/P ratio of 1.03, and with an N/P ratio of 1.03 and 0.08% BSA, both show statistically significant differences ($p < 0.0001$) in cell viability, with viabilities of 93% for N/P 1.03, and 90% for N/P 1.03 with 0.08% BSA. The difference in viability between the N/P 1.03 complexes with and without 0.08% BSA was not significant (ns), indicating that the addition of BSA did not significantly alter the toxicity profile. At 72 h, the complexes with an N/P ratio of 1.03 exhibited a slight decrease in viability, from 95% to 93%, indicating a minor impact on cell viability ($p = 0.056$). The complexes formulated considering an N/P ratio of 1.03 and 0.08% BSA led to a cellular viability of 91% ($p < 0.0001$ for the comparison with the control cells). The viability for the non-BSA-coated counterpart was 93%.

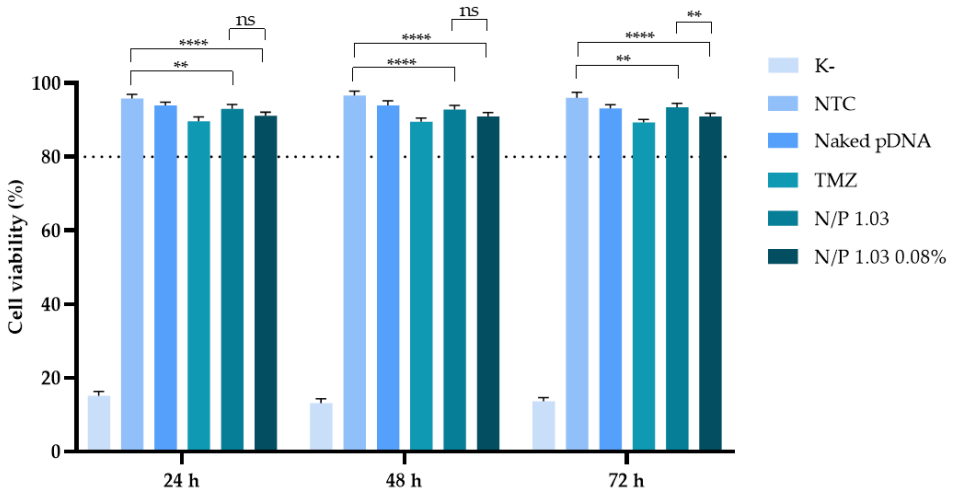

Figure 18. Cellular viability of HA1800 cells after 24 h, 48 h, and 72 h of incubation with the optimal BSA-free and BSA-coated TMZ-WRAP5/p53 complexes (0.1 µg of pDNA per well, N/P 1.03 and 0.08% BSA). Cells treated with ethanol were used as negative control (K–), and non-transfected cells were used as positive control (K+). Statistical analysis was completed using one-way ANOVA with data obtained from six independent measurements (mean ± SD, n = 6). (**** $p \leq 0.0001$; ** $p \leq 0.01$). ns—statistically non-significant.

Although there are statistical significant differences between the control cells and the TMZ-WRAP5/p53 complexes, this study revealed that the optimal BSA coated TMZ-WRAP5/p53 complexes do not induce any toxic effects on normal brain cells, as the obtained values for the cellular viability remained above 80%, what is in line with the non-toxic nature of the compounds according to ISO 10993-5 [222]. The preservation of astrocyte viability in the presence of these nanocomplexes suggests that they are non-toxic to brain cells, which is relevant to ensure protection of healthy brain cells.

4.9. Hemocompatibility

The hemocompatibility of the optimal point, with and without BSA, was evaluated through a hemolysis test by incubation of TMZ-WRAP5/p53 complexes in rat blood cells. Figure 19 summarizes the obtained results. The nanocomplexes without BSA had a hemolysis rate of 5.9%, exceeding the threshold for non-hemolytic materials (5%). However, after adding BSA as a coating, the hemolysis rate decreased to 3.9%. BSA, being a stable protein compatible with the human body, minimizes the potential for triggering an adverse immune or inflammatory response that could contribute to hemolysis. None of the developed peptide nanocomplexes, however, exhibited statistically significant differences compared to the negative control, further reinforcing the absence of hemolysis.

These results demonstrated the non-hemocompatible behavior of the optimal BSA-coated TMZ-WRAP5/p53 nanocomplexes.

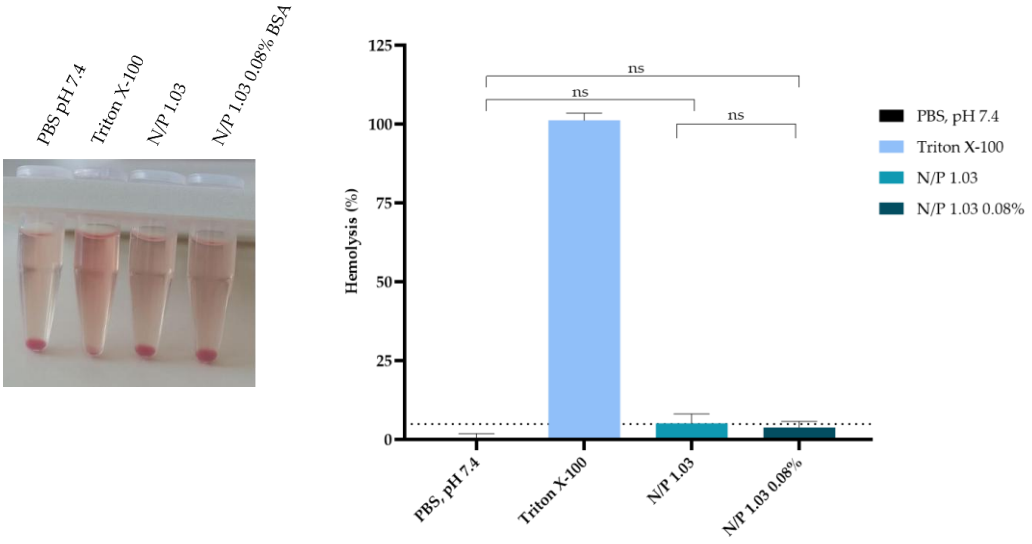

Figure 19. *In vitro* hemolysis assay was performed on rat red blood cells (RBCs), which were incubated with the optimal BSA-free and BSA-coated TMZ-WRAP5/p53 complexes (1 µg of pDNA, N/P ratio = 1.03). PBS pH 7.4 was considered as the negative control, while in the positive control, RBCs were incubated with Triton X-100 (10%) to provoke hemolysis. Statistical analysis was completed using one-way ANOVA with data obtained from three independent measurements (mean ± SD, n = 3). ns—statistically non-significant.

4.10. Glioblastoma cytotoxicity

The p53 mRNA transcription in U-87 cells 24 h after transfection with the optimal BSA-coated TMZ-WRAP5/p53 complexes has been evaluated by RT-PCR assay with p53 specific primers. Non-transfected cells, cells transfected with naked pDNA, and cells transfected with TMZ alone were used as controls. The results are presented in Figure 20 and show significant levels of mRNA of p53 for both optimal BSA-free and BSA-coated TMZ-WRAP5/p53 complexes (band at 150 bp), demonstrating the efficiency of both complexes to induce gene transcription in glioblastoma cells. A more intense band from p53 transcripts can, however, be observed for the transfection carried out by the optimal BSA-coated complexes suggesting higher levels of mRNA. Although a deep investigation into the synergistic effect is mandatory to unravel the cancer therapeutic effect of the optimal BSA-coated TMZ-WRAP5/p53, data from Figure 20 give a first insight into their potential to mediate co-delivery against glioblastoma.

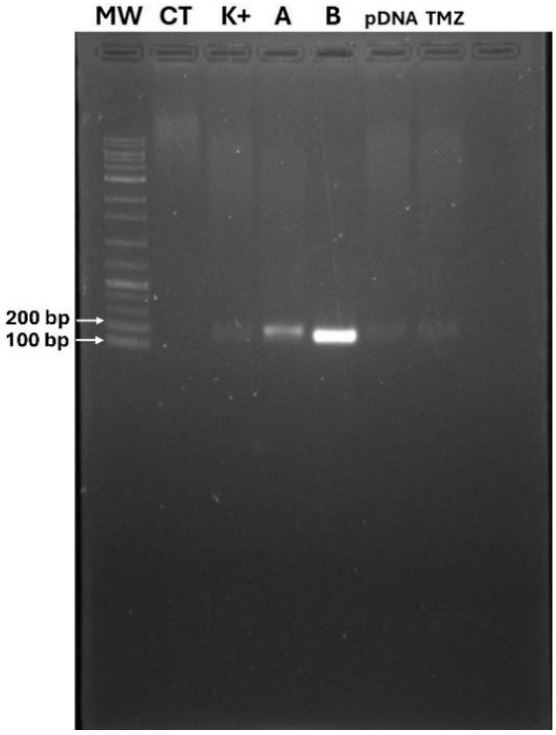

Figure 20. PCR analysis of p53 mRNA in U-87 cells after 24 h of transfection mediated by A - optimal BSA-free and B - BSA-coated TMZ-WRAP5/p53 complexes (1 μg of pDNA, N/P ratio = 1.03). MW - DNA ladder molecular weight marker; CT – control without cDNA sample.

The quantification of p53 expression through quantitative PCR (qPCR) at 24 h revealed significant differences in p53 levels between the complexes. The data presented in Figure 21 show that both the TMZ-WRAP5/pDNA complex and the BSA-coated TMZ-WRAP5/pDNA complex led to notable increases in p53 expression compared to untransfected control cells. Specifically, the TMZ-WRAP5/pDNA complex resulted in a 55.4-fold increase ($p<0.0001$) in p53 expression, demonstrating its ability to efficiently deliver the p53 gene and induce its expression in glioblastoma cells. However, the BSA-coated TMZ-WRAP5/pDNA complex exhibited an even

more significant effect, with an 82.6-fold increase ($p<0.0001$) in p53 expression, showing a higher transfection efficiency when BSA was present. Furthermore, a direct comparison between the two complexes revealed a statistically significant difference ($p<0.0001$), with the BSA-coated complex producing higher levels of p53 expression than the uncoated system. These results are consistent with those observed in conventional PCR experiments, which also indicated a significant trend toward increased p53 production when glioblastoma cells were exposed to the BSA-coated complex. This suggests that the BSA coating not only improves the delivery of the complex but also enhances the overall effectiveness of the system in inducing p53 gene expression, which is crucial for triggering tumor-suppressive responses in glioblastoma cells.

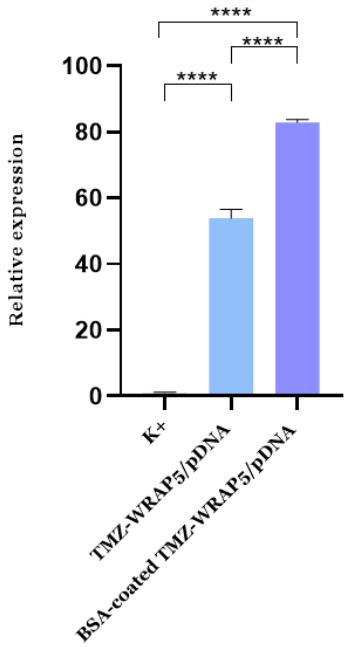

Figure 21. qPCR analysis of relative expression of p53 mRNA in U-87 cells 24 hours after transfection with TMZ-WRAP5/pDNA and BSA-coated TMZ-WRAP5/pDNA complexes. Untransfected cells (K+) were used as control. Statistical analysis was completed using one-way ANOVA.

PCR results showing a significant increase in p53 production after exposure to BSA-containing complexes in glioblastoma cells highlight the potential of BSA as an enhancer in therapeutic delivery systems.

The data from an MTT study performed at 24, 48 and 72 h post-transfection are summarized in Figure 22. Independently of the time considered, all samples exhibited statistically significant differences in comparison with the positive control, ****$p \leq 0.0001$, demonstrating an induced effect on the viability of U-87 cells. The reduction in the cellular viability is particularly accentuated for the transfection mediated by the optimal BSA-free and BSA-coated TMZ-WRAP5/p53 complexes, and the extent of this phenomenon increases with the time of transfection. The results also demonstrated that the BSA-coated complexes were able to promote a higher decrease in U-87 cells viability when compared to the effect produced by the correspondent BSA free complexes at 24 h (**$p \leq 0.001$) and 48 h (*$p \leq 0.05$). The difference on

viability between BSA-free and BSA-coated TMZ-WRAP5/p53 complexes was, however, not statistically significant at 72 h post-transfection.

As the nanocomplexes demonstrated to be biocompatible to normal astrocyte cells, the observed decrease in U-87 cells viability may be related with the apoptosis effect induced by p53 gene expression mediated by the nanocomplexes and by the action of TMZ. Therefore, we can correlate the obtained data on U-87 cells with efficient transfection, p53 gene expression and apoptotic effects from the combined action of p53 and TMZ.

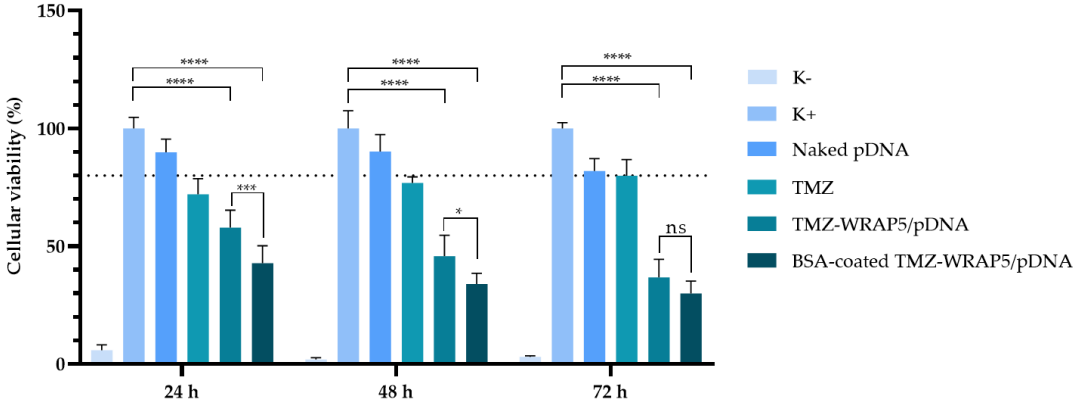

Figure 22. Cellular viability of U87 cells after 24 h, 48 h, and 72 h of incubation with the optimal BSA-free and BSA-coated TMZ-WRAP5/p53 complexes (0.1 µg of pDNA per well, N/P 1.03 and 0.08% BSA). Cells treated with ethanol were used as negative control (K-)

The presence of BSA in nanoparticle complexes has a significant impact on their effectiveness in treating glioblastoma cells, as evidenced by the decrease in cell viability at 24 and 72 hours compared to the complex without BSA. This may be due to the fact that BSA's role as a stabilizing agent is crucial for maintaining the structural integrity of nanoparticles in biological environments because, by forming a protein corona, BSA prevents aggregation and improves the stability of nanoparticles, increasing their ability to reach glioblastoma cells intact [223]. In addition, BSA reduces non-specific interactions with serum proteins and immune cells, minimizing elimination by the mononuclear phagocytic system and prolonging circulation time, which further increases delivery efficacy [223]. Glioblastoma cells overexpress albumin-binding proteins, gp60 and SPARC, which BSA-coated nanoparticles can exploit for receptor-mediated endocytosis [223]. This targeting mechanism allows the nanoparticles to selectively enter glioblastoma cells, maximizing therapeutic efficacy [223]. The BSA coating also plays a role in facilitating penetration through the blood-brain barrier (BBB) as the BSA-coated complexes can access the brain parenchyma and reach the glioblastoma cells more effectively [224].

Chapter 5- Conclusions and Future Perspectives

Cancer remains one of the most challenging and lethal diseases confronting humanity. Traditional cancer treatments, such as surgery, radiotherapy, and chemotherapy, often prove insufficient, and they are frequently accompanied by numerous adverse side effects. Consequently, researchers continue to explore alternative and innovative treatment approaches. Glioblastoma therapy urgently seeks innovative and effective strategies to enhance clinical outcomes, with combined chemo- and gene therapies showing substantial promise. This study employed Design of Experiments to swiftly and accurately identify the most effective BSA-coated TMZ-WRAP5/p53 gene-based pDNA complexes for co-delivery to glioma cells. The DoE approach optimized key formulation variables, including N/P ratio, BSA concentration, and BSA coating time (as a categorical variable), with particle size, polydispersity index, surface charge, and pDNA complexation capacity as outputs.

The derived quadratic models were statistically robust, with a non-significant lack of fit and strong predictive values ($R^2 > 0.84$, adjusted $R^2 > 0.88$, and predicted $R^2 > 0.72$), indicating a well-fitting model. The optimal formulation, confirmed experimentally, was achieved with an N/P ratio of 1.03 and a BSA concentration of 0.08%, added 25 min post-formulation. This formulation produced nanocomplexes with an average size of approximately 182 nm, a zeta potential of +9.8 mV, and a pDNA CC of 96.5%. Morphologically, these complexes were spherical, biocompatible with human astrocytes, stable in cell culture media and serum, and effectively protected pDNA from degradation.

The optimal BSA-coated TMZ-WRAP5/p53 complexes were shown to be hemocompatible and biocompatible, underscoring their potential for safe *in vivo* applications. Importantly, they demonstrated efficient gene transcription and significantly reduced U-87 cell viability. This work confirms DoE as a powerful tool for identifying optimal formulations, revealing highly promising BSA-coated TMZ-WRAP5/p53 nanocomplexes for synergistic chemo-gene delivery in glioblastoma therapy, setting a strong foundation for further in-depth *in vitro* research.

The promising results of this study open up several interesting avenues for future research. Next steps include evaluating the therapeutic efficacy of these nanocomplexes in more advanced *in vitro* glioblastoma models, such as 3D spheroids, to better mimic the tumor microenvironment and validate their antitumor potential. *In vivo* studies using glioblastoma animal models will be crucial to evaluate its biodistribution, pharmacokinetics and long-term safety profiles, providing information on its systemic behavior and therapeutic window. These studies will aim to determine the nanocomplexes' ability to effectively target glioblastoma cells, minimizing off-target effects. It is hoped that these investigations will further establish the viability of this approach for clinical translation, ultimately offering a more effective and targeted therapeutic option for glioblastoma patients.

Chapter 6- Bibliography

1. Saini, A., et al., *Cancer causes and treatments*. Int. J. Pharm. Sci. Res, 2020. **11**: p. 3121-3134.
2. Fares, J., et al., *Molecular principles of metastasis: a hallmark of cancer revisited*. Signal Transduction and Targeted Therapy, 2020. **5**(1): p. 28.
3. Hanahan, D. and R.A. Weinberg, *Hallmarks of cancer: the next generation*. Cell, 2011. **144**(5): p. 646-74.
4. Vogelstein, B., et al., *Cancer genome landscapes*. Science, 2013. **339**(6127): p. 1546-58.
5. Kim, J.W., et al., *Genes with dual proto-oncogene and tumor suppressor gene activities are frequently altered by protein losses in colon cancers*. Pathology - Research and Practice, 2023. **248**: p. 154659.
6. Kontomanolis, E.N., et al., *Role of Oncogenes and Tumor-suppressor Genes in Carcinogenesis: A Review*. Anticancer Research, 2020. **40**(11): p. 6009.
7. Kang, Z., Q. Yang, and Y. Li, *DNA Repair in Cancer*. J Oncol, 2019. **2019**: p. 8676947.
8. Kiwerska, K. and K. Szyfter, *DNA repair in cancer initiation, progression, and therapy-a double-edged sword*. J Appl Genet, 2019. **60**(3-4): p. 329-334.
9. Kim, S.K. and S.W. Cho, *The Evasion Mechanisms of Cancer Immunity and Drug Intervention in the Tumor Microenvironment*. Front Pharmacol, 2022. **13**: p. 868695.
10. Abate, M., et al., *Psychological Stress and Cancer: New Evidence of An Increasingly Strong Link*. Transl Med UniSa, 2020. **23**: p. 53-57.
11. Falcinelli, M., et al., *The Role of Psychologic Stress in Cancer Initiation: Clinical Relevance and Potential Molecular Mechanisms*. Cancer Res, 2021. **81**(20): p. 5131-5140.
12. Moutinho, B.D., et al., *Immunosuppression and Malignant Neoplasms: Risk-Benefit Assessment in Patients with Inflammatory Bowel Disease*. Am J Case Rep, 2020. **21**: p. e920949.
13. Rashidian, H., et al., *An Ecological Study of the Association between Opiate Use and Incidence of Cancers*. Addict Health, 2016. **8**(4): p. 252-260.
14. Martínez-Reyes, I. and N.S. Chandel, *Cancer metabolism: looking forward*. Nature Reviews Cancer, 2021. **21**(10): p. 669-680.
15. Senga, S.S. and R.P. Grose, *Hallmarks of cancer-the new testament*. Open Biol, 2021. **11**(1): p. 200358.
16. Li, C., et al., *Metabolic reprogramming in cancer cells: glycolysis, glutaminolysis, and Bcl-2 proteins as novel therapeutic targets for cancer*. World Journal of Surgical Oncology, 2016. **14**(1): p. 15.
17. Gyamfi, J., J. Kim, and J. Choi, *Cancer as a Metabolic Disorder*. International Journal of Molecular Sciences, 2022. **23**(3): p. 1155.
18. DeBerardinis, R.J. and N.S. Chandel, *Fundamentals of cancer metabolism*. Sci Adv, 2016. **2**(5): p. e1600200.
19. Liberti, M.V. and J.W. Locasale, *The Warburg Effect: How Does it Benefit Cancer Cells?* Trends in Biochemical Sciences, 2016. **41**(3): p. 211-218.
20. Chandel, N.S., *Glycolysis*. Cold Spring Harb Perspect Biol, 2021. **13**(5).
21. Lebelo, M.T., A.M. Joubert, and M.H. Visagie, *Warburg effect and its role in tumourigenesis*. Archives of Pharmacal Research, 2019. **42**(10): p. 833-847.
22. Martinez-Outschoorn, U.E., et al., *Cancer metabolism: a therapeutic perspective*. Nature Reviews Clinical Oncology, 2017. **14**(1): p. 11-31.
23. Schiliro, C. and B.L. Firestein, *Mechanisms of Metabolic Reprogramming in Cancer Cells Supporting Enhanced Growth and Proliferation*. Cells, 2021. **10**(5).
24. Jiang, M., H. Fang, and H. Tian, *Metabolism of cancer cells and immune cells in the initiation, progression, and metastasis of cancer*. Theranostics, 2025. **15**(1): p. 155-188.

25. Guan, X., *Cancer metastases: challenges and opportunities*. Acta Pharmaceutica Sinica B, 2015. **5**(5): p. 402-418.
26. Rajabi, M. and S.A. Mousa *The Role of Angiogenesis in Cancer Treatment*. Biomedicines, 2017. **5**, DOI: 10.3390/biomedicines5020034.
27. Liu, Z.-L., et al., *Angiogenic signaling pathways and anti-angiogenic therapy for cancer*. Signal Transduction and Targeted Therapy, 2023. **8**(1): p. 198.
28. Kazerounian, S. and J. Lawler, *Integration of pro- and anti-angiogenic signals by endothelial cells*. Journal of Cell Communication and Signaling, 2018. **12**(1): p. 171-179.
29. Al-Ostoot, F.H., et al., *Tumor angiogenesis: Current challenges and therapeutic opportunities*. Cancer Treatment and Research Communications, 2021. **28**: p. 100422.
30. Zuo, J., et al., *Hypoxia promotes the invasion and metastasis of laryngeal cancer cells via EMT*. Medical Oncology, 2016. **33**(2): p. 15.
31. Lv, X., et al., *The role of hypoxia-inducible factors in tumor angiogenesis and cell metabolism*. Genes & Diseases, 2017. **4**(1): p. 19-24.
32. Lawler, J., *Counter regulation of tumor angiogenesis by vascular endothelial growth factor and thrombospondin-1*. Seminars in Cancer Biology, 2022. **86**: p. 126-135.
33. Nenclares, P. and K.J. Harrington, *The biology of cancer*. Medicine, 2020. **48**(2): p. 67-72.
34. Isenberg, J.S. and D.D. Roberts, *THBS1 (thrombospondin-1)*. Atlas Genet Cytogenet Oncol Haematol, 2020. **24**(8): p. 291-299.
35. Lowe, S.W. and A.W. Lin, *Apoptosis in cancer*. Carcinogenesis, 2000. **21**(3): p. 485-495.
36. Morana, O., W. Wood, and C.D. Gregory *The Apoptosis Paradox in Cancer*. International Journal of Molecular Sciences, 2022. **23**, DOI: 10.3390/ijms23031328.
37. Kiraz, Y., et al., *Major apoptotic mechanisms and genes involved in apoptosis*. Tumor Biology, 2016. **37**(7): p. 8471-8486.
38. Singh, P. and B. Lim, *Targeting Apoptosis in Cancer*. Current Oncology Reports, 2022. **24**(3): p. 273-284.
39. Yanumula, A. and J.K. Cusick, *Biochemistry, Extrinsic Pathway of Apoptosis*. 2023: StatPearls Publishing, Treasure Island (FL).
40. Tummers, B. and D.R. Green, *Caspase-8: regulating life and death*. Immunological Reviews, 2017. **277**(1): p. 76-89.
41. Asadi, M., et al., *Caspase-3: Structure, function, and biotechnological aspects*. Biotechnology and Applied Biochemistry, 2022. **69**(4): p. 1633-1645.
42. Redza-Dutordoir, M. and D.A. Averill-Bates, *Activation of apoptosis signalling pathways by reactive oxygen species*. Biochimica et Biophysica Acta (BBA) - Molecular Cell Research, 2016. **1863**(12): p. 2977-2992.
43. Shakeri, R., A. Kheirollahi, and J. Davoodi, *Contribution of Apaf-1 to the pathogenesis of cancer and neurodegenerative diseases*. Biochimie, 2021. **190**: p. 91-110.
44. Liao, D., *Chapter 1 - Apoptosis, necroptosis, and pyroptosis in health and disease: an overview of molecular mechanisms, targets for therapeutic development, and known small molecule and biologic modulators*, in *Mechanisms of Cell Death and Opportunities for Therapeutic Development*, D. Liao, Editor. 2022, Academic Press. p. 1-46.
45. Neves, A., et al. *Evidence That a Peptide-Drug/p53 Gene Complex Promotes Cognate Gene Expression and Inhibits the Viability of Glioblastoma Cells*. Pharmaceutics, 2024. **16**, DOI: 10.3390/pharmaceutics16060781.
46. Wirsching, H.-G. and M. Weller, *Glioblastoma*, in *Malignant Brain Tumors : State-of-the-Art Treatment*, J. Moliterno Gunel, J.M. Piepmeier, and J.M. Baehring, Editors. 2017, Springer International Publishing: Cham. p. 265-288.

47. Mohammed, S., M. Dinesan, and T. Ajayakumar, *Survival and quality of life analysis in glioblastoma multiforme with adjuvant chemoradiotherapy: a retrospective study*. Rep Pract Oncol Radiother, 2022. **27**(6): p. 1026-1036.
48. Grochans, S., et al. *Epidemiology of Glioblastoma Multiforme–Literature Review*. Cancers, 2022. **14**, DOI: 10.3390/cancers14102412.
49. Masui, K., P.S. Mischel, and G. Reifenberger, *Chapter 6 - Molecular classification of gliomas*, in *Handbook of Clinical Neurology*, M.S. Berger and M. Weller, Editors. 2016, Elsevier. p. 97-120.
50. Perrin, S.L., et al., *Glioblastoma heterogeneity and the tumour microenvironment: implications for preclinical research and development of new treatments*. Biochem Soc Trans, 2019. **47**(2): p. 625-638.
51. Wirsching, H.-G., E. Galanis, and M. Weller, *Chapter 23 - Glioblastoma*, in *Handbook of Clinical Neurology*, M.S. Berger and M. Weller, Editors. 2016, Elsevier. p. 381-397.
52. Angom, R.S., N.M.R. Nakka, and S. Bhattacharya, *Advances in Glioblastoma Therapy: An Update on Current Approaches*. Brain Sci, 2023. **13**(11).
53. Sahoo, O.S., R. Mitra, and N.K.H. Nagaiah, *The hidden architects of glioblastoma multiforme: Glioma stem cells*. MedComm – Oncology, 2024. **3**(1): p. e66.
54. Rominiyi, O. and S.J. Collis, *DDRugging glioblastoma: understanding and targeting the DNA damage response to improve future therapies*. Mol Oncol, 2022. **16**(1): p. 11-41.
55. Ahmed, M.H., et al., *Overcoming the blood brain barrier in glioblastoma: Status and future perspective*. Rev Neurol (Paris), 2023. **179**(5): p. 430-436.
56. Li, R., et al., *Genetic and clinical characteristics of primary and secondary glioblastoma is associated with differential molecular subtype distribution*. Oncotarget, 2015. **6**(9): p. 7318-24.
57. Hanif, F., et al., *Glioblastoma Multiforme: A Review of its Epidemiology and Pathogenesis through Clinical Presentation and Treatment*. Asian Pac J Cancer Prev, 2017. **18**(1): p. 3-9.
58. Sarkar, S. and S. Patranabis, *Immunomodulatory signalling networks in glioblastoma multiforme: a comprehensive review of therapeutic approaches*. Human Cell, 2024.
59. Yoshikawa, M.H., et al., *Modifiable risk factors for glioblastoma: a systematic review and meta-analysis*. Neurosurgical Review, 2023. **46**(1): p. 143.
60. Wiedmann, M.K.H., et al., *The impact of body mass index and height on the risk for glioblastoma and other glioma subgroups: a large prospective cohort study*. Neuro Oncol, 2017. **19**(7): p. 976-985.
61. Baglietto, L., et al., *Alcohol consumption and risk of glioblastoma; evidence from the Melbourne collaborative cohort study*. International Journal of Cancer, 2011. **128**(8): p. 1929-1934.
62. Cote, D.J., et al., *Alcohol intake and risk of glioma: results from three prospective cohort studies*. European Journal of Epidemiology, 2021. **36**(9): p. 965-974.
63. Villeneuve, P.J., et al., *Brain cancer and occupational exposure to magnetic fields among men: results from a Canadian population-based case-control study*. International Journal of Epidemiology, 2002. **31**(1): p. 210-217.
64. Thériault, G., et al., *Cancer Risks Associated with Occupational Exposure to Magnetic Fields among Electric Utility Workers in Ontario and Quebec, Canada, and France: 1970–1989*. American Journal of Epidemiology, 1994. **139**(6): p. 550-572.
65. Daugherty, S.E., et al., *Nonsteroidal Anti-inflammatory Drugs and Glioma in the NIH-AARP Diet and Health Study Cohort*. Cancer Prevention Research, 2011. **4**(12): p. 2027-2034.
66. Scheurer, M.E., et al., *Effects of antihistamine and anti-inflammatory medication use on risk of specific glioma histologies*. International Journal of Cancer, 2011. **129**(9): p. 2290-2296.

67. Sivak-Sears, N.R., et al., *Case-Control Study of Use of Nonsteroidal Antiinflammatory Drugs and Glioblastoma Multiforme*. American Journal of Epidemiology, 2004. **159**(12): p. 1131-1139.
68. Schüz, J., et al., *European Code against Cancer 4th Edition: 12 ways to reduce your cancer risk*. Cancer Epidemiology, 2015. **39**: p. S1-S10.
69. Ba, S., et al., *Diet, nutrition and the prevention of excess weight gain and obesity*. Public Health Nutrition, 2004. **7**(1a): p. 123-146.
70. Gray, A., et al., *A review of nutrition and dietary interventions in oncology*. SAGE Open Medicine, 2020. **8**: p. 2050312120926877.
71. Key, T.J., et al., *Diet, nutrition and the prevention of cancer*. Public Health Nutrition, 2004. **7**(1a): p. 187-200.
72. Guasch-Ferré, M. and W.C. Willett, *The Mediterranean diet and health: a comprehensive overview*. J Intern Med, 2021. **290**(3): p. 549-566.
73. Misiąg, W., et al., *Physical Activity and Cancer Care—A Review*. Cancers, 2022. **14**(17): p. 4154.
74. Caliri, A.W., S. Tommasi, and A. Besaratinia, *Relationships among smoking, oxidative stress, inflammation, macromolecular damage, and cancer*. Mutation Research/Reviews in Mutation Research, 2021. **787**: p. 108365.
75. Rumgay, H., et al., *Alcohol and Cancer: Epidemiology and Biological Mechanisms*. Nutrients, 2021. **13**(9): p. 3173.
76. Michalak, A., T. Lach, and H. Cichoż-Lach, *Oxidative Stress—A Key Player in the Course of Alcohol-Related Liver Disease*. Journal of Clinical Medicine, 2021. **10**(14): p. 3011.
77. Guo, C., et al., *Adjuvant Temozolomide Chemotherapy With or Without Interferon Alfa Among Patients With Newly Diagnosed High-grade Gliomas: A Randomized Clinical Trial*. JAMA Netw Open, 2023. **6**(1): p. e2253285.
78. Bhaskaran, D., et al., *A randomised phase II trial of temozolomide with or without cannabinoids in patients with recurrent glioblastoma (ARISTOCRAT): protocol for a multi-centre, double-blind, placebo-controlled trial*. BMC Cancer, 2024. **24**(1): p. 83.
79. Ortiz, R., et al., *Temozolomide: An Updated Overview of Resistance Mechanisms, Nanotechnology Advances and Clinical Applications*. Curr Neuropharmacol, 2021. **19**(4): p. 513-537.
80. Zhang, J., M. F.G. Stevens, and T. D. Bradshaw, *Temozolomide: Mechanisms of Action, Repair and Resistance*. Current Molecular Pharmacology, 2012. **5**(1): p. 102-114.
81. Barciszewska, A.M., et al., *A New Epigenetic Mechanism of Temozolomide Action in Glioma Cells*. PLoS One, 2015. **10**(8): p. e0136669.
82. Aleksakhina, S.N., A. Kashyap, and E.N. Imyanitov, *Mechanisms of acquired tumor drug resistance*. Biochimica et Biophysica Acta (BBA) - Reviews on Cancer, 2019. **1872**(2): p. 188310.
83. Zhang, J., M.F. Stevens, and T.D. Bradshaw, *Temozolomide: mechanisms of action, repair and resistance*. Curr Mol Pharmacol, 2012. **5**(1): p. 102-14.
84. Messaoudi, K., A. Clavreul, and F. Lagarce, *Toward an effective strategy in glioblastoma treatment. Part I: resistance mechanisms and strategies to overcome resistance of glioblastoma to temozolomide*. Drug Discovery Today, 2015. **20**(7): p. 899-905.
85. Fan, C.H., et al., *O6-methylguanine DNA methyltransferase as a promising target for the treatment of temozolomide-resistant gliomas*. Cell Death & Disease, 2013. **4**(10): p. e876-e876.
86. Wick, W., et al., *MGMT testing—the challenges for biomarker-based glioma treatment*. Nature Reviews Neurology, 2014. **10**(7): p. 372-385.
87. Chai, R., et al., *Predictive value of MGMT promoter methylation on the survival of TMZ treated IDH-mutant glioblastoma*. Cancer Biol Med, 2021. **18**(1): p. 272-282.

88. Butler, M., et al., *MGMT Status as a Clinical Biomarker in Glioblastoma*. Trends Cancer, 2020. **6**(5): p. 380-391.
89. Catalano, A., et al. *Multidrug Resistance (MDR): A Widespread Phenomenon in Pharmacological Therapies*. Molecules, 2022. **27**, DOI: 10.3390/molecules27030616.
90. Wang, D., et al., *A comprehensive review in improving delivery of small-molecule chemotherapeutic agents overcoming the blood-brain/brain tumor barriers for glioblastoma treatment*. Drug Delivery, 2019. **26**(1): p. 551-565.
91. Zhao, S., S. Tadesse, and D. Kidane, *Chapter Four - Significance of base excision repair to human health*, in *International Review of Cell and Molecular Biology*, U. Weyemi and L. Galluzzi, Editors. 2021, Academic Press. p. 163-193.
92. Agnihotri, S., et al., *Alkylpurine-DNA-N-glycosylase confers resistance to temozolomide in xenograft models of glioblastoma multiforme and is associated with poor survival in patients*. J Clin Invest, 2012. **122**(1): p. 253-66.
93. Talukdar, S., et al., *Chapter Four - EGFR: An essential receptor tyrosine kinase-regulator of cancer stem cells*, in *Advances in Cancer Research*, R. Kumar and P.B. Fisher, Editors. 2020, Academic Press. p. 161-188.
94. El Khayari, A., et al., *Metabolic Rewiring in Glioblastoma Cancer: EGFR, IDH and Beyond*. Frontiers in Oncology, 2022. **12**.
95. Rodriguez, S.M., et al. *An Overview of EGFR Mechanisms and Their Implications in Targeted Therapies for Glioblastoma*. International Journal of Molecular Sciences, 2023. **24**, DOI: 10.3390/ijms241311110.
96. Song, Y., et al., *Targeting RAS–RAF–MEK–ERK signaling pathway in human cancer: Current status in clinical trials*. Genes & Diseases, 2023. **10**(1): p. 76-88.
97. Guda, M.R., et al., *Galectin-1 activates carbonic anhydrase IX and modulates glioma metabolism*. Cell Death & Disease, 2022. **13**(6): p. 574.
98. Ko, F.C., et al. *Chimera and Tandem-Repeat Type Galectins: The New Targets for Cancer Immunotherapy*. Biomolecules, 2023. **13**, DOI: 10.3390/biom13060902.
99. Danhier, F., et al., *Combined anti-Galectin-1 and anti-EGFR siRNA-loaded chitosan-lipid nanocapsules decrease temozolomide resistance in glioblastoma: In vivo evaluation*. International Journal of Pharmaceutics, 2015. **481**(1): p. 154-161.
100. Feroz, W. and A.M.A. Sheikh, *Exploring the multiple roles of guardian of the genome: P53*. Egyptian Journal of Medical Human Genetics, 2020. **21**(1): p. 49.
101. Ali, G. and B.S. Ahmed, *Mechanism of Action p53*. Egyptian Journal of Veterinary Sciences, 2023. **54**(5): p. 941-948.
102. Lang, F., et al., *Genotoxic therapy and resistance mechanism in gliomas*. Pharmacology & Therapeutics, 2021. **228**: p. 107922.
103. Olafson, L.R., et al., *The role of TP53 gain-of-function mutation in multifocal glioblastoma*. Journal of Neuro-Oncology, 2020. **147**(1): p. 37-47.
104. Zhang, Y., et al. *The p53 Pathway in Glioblastoma*. Cancers, 2018. **10**, DOI: 10.3390/cancers10090297.
105. Stark, A.M., et al., *p53, mdm2, EGFR, and msh2 expression in paired initial and recurrent glioblastoma multiforme*. Journal of Neurology, Neurosurgery & Psychiatry, 2003. **74**(6): p. 779.
106. Pellot Ortiz, K.I., et al., *MDM2 Inhibition in the Treatment of Glioblastoma: From Concept to Clinical Investigation*. Biomedicines, 2023. **11**(7): p. 1879.
107. Pellot Ortiz, K.I., et al. *MDM2 Inhibition in the Treatment of Glioblastoma: From Concept to Clinical Investigation*. Biomedicines, 2023. **11**, DOI: 10.3390/biomedicines11071879.
108. Lefranc, F., et al., *Present and potential future adjuvant issues in high-grade astrocytic glioma treatment*. Adv Tech Stand Neurosurg, 2009. **34**: p. 3-35.
109. Carnero, A., et al., *The PTEN/PI3K/AKT signalling pathway in cancer, therapeutic implications*. Current cancer drug targets, 2008. **8**(3): p. 187-198.

110. Mukherjee, R., et al., *Regulation of PTEN translation by PI3K signaling maintains pathway homeostasis.* Molecular Cell, 2021. **81**(4): p. 708-723.e5.
111. O'Brien, M.A. and R. Kirby, *Apoptosis: A review of pro-apoptotic and anti-apoptotic pathways and dysregulation in disease.* Journal of veterinary emergency and critical care, 2008. **18**(6): p. 572-585.
112. Sweeney, M.D., et al., *Blood-brain barrier: from physiology to disease and back.* Physiological reviews, 2018.
113. Wu, D., et al., *The blood–brain barrier: Structure, regulation and drug delivery.* Signal Transduction and Targeted Therapy, 2023. **8**(1): p. 217.
114. Krajcer, A., E. Grzywna, and J. Lewandowska-Łańcucka, *Strategies increasing the effectiveness of temozolomide at various levels of anti-GBL therapy.* Biomedicine & Pharmacotherapy, 2023. **165**: p. 115174.
115. Gerber, D.E., *Targeted therapies: a new generation of cancer treatments.* Am Fam Physician, 2008. **77**(3): p. 311-9.
116. Schirrmacher, V., *From chemotherapy to biological therapy: A review of novel concepts to reduce the side effects of systemic cancer treatment (Review).* Int J Oncol, 2019. **54**(2): p. 407-419.
117. Yahya, E.B. and A.M. Alqadhi, *Recent trends in cancer therapy: A review on the current state of gene delivery.* Life Sciences, 2021. **269**: p. 119087.
118. Ramamoorth, M. and A. Narvekar, *Non viral vectors in gene therapy- an overview.* J Clin Diagn Res, 2015. **9**(1): p. Ge01-6.
119. Taghdiri, M. and C. Mussolino *Viral and Non-Viral Systems to Deliver Gene Therapeutics to Clinical Targets*. International Journal of Molecular Sciences, 2024. **25**, DOI: 10.3390/ijms25137333.
120. Papanikolaou, E. and A. Bosio, *The promise and the hope of gene therapy.* Frontiers in genome editing, 2021. **3**: p. 618346.
121. Dunbar, C.E., et al., *Gene therapy comes of age.* Science, 2018. **359**(6372): p. eaan4672.
122. Sheykhhasan, M., et al., *Could gene therapy cure HIV?* Life Sciences, 2021. **277**: p. 119451.
123. Uddin, F., C.M. Rudin, and T. Sen, *CRISPR gene therapy: applications, limitations, and implications for the future.* Frontiers in oncology, 2020. **10**: p. 1387.
124. Zhao, Z., A.C. Anselmo, and S. Mitragotri, *Viral vector-based gene therapies in the clinic.* Bioengineering & translational medicine, 2022. **7**(1): p. e10258.
125. Sayed, N., et al., *Gene therapy: Comprehensive overview and therapeutic applications.* Life sciences, 2022. **294**: p. 120375.
126. Lowenstein, P.R. and M.G. Castro, *Inflammation and adaptive immune responses to adenoviral vectors injected into the brain: peculiarities, mechanisms, and consequences.* Gene Therapy, 2003. **10**(11): p. 946-954.
127. Shrivastava, V., N. Nama, and M. Gupta, *A review on Adenovirus.* 2022.
128. Chen, Y.H., M.S. Keiser, and B.L. Davidson, *Viral Vectors for Gene Transfer.* Current Protocols in Mouse Biology, 2018. **8**(4): p. e58.
129. Desheva, Y., *Introductory chapter: Human adenoviruses*, in *Adenoviruses.* 2018, IntechOpen.
130. Wold, W.S. and K. Toth, *Adenovirus vectors for gene therapy, vaccination and cancer gene therapy.* Curr Gene Ther, 2013. **13**(6): p. 421-33.
131. Fu, Q., et al., *Critical challenges and advances in recombinant adeno-associated virus (rAAV) biomanufacturing.* Biotechnology and Bioengineering, 2023. **120**(9): p. 2601-2621.
132. Qu, Y., et al., *Characteristics and advantages of adeno-associated virus vector-mediated gene therapy for neurodegenerative diseases.* Neural Regeneration Research, 2019. **14**(6).

133. Song, L., R.J. Samulski, and M.L. Hirsch, *Adeno-associated virus vector mobilization, risk versus reality*. Human gene therapy, 2020. **31**(19-20): p. 1054-1067.
134. Hanson, H.M., et al., *Human Retrovirus Genomic RNA Packaging*. Viruses, 2022. **14**(5): p. 1094.
135. Yoder, K.E., et al., *Strategies for targeting retroviral integration for safer gene therapy: advances and challenges*. Frontiers in Molecular Biosciences, 2021. **8**: p. 662331.
136. Butt, M.H., et al. *Appraisal for the Potential of Viral and Nonviral Vectors in Gene Therapy: A Review*. Genes, 2022. **13**, DOI: 10.3390/genes13081370.
137. Zu, H. and D. Gao, *Non-viral vectors in gene therapy: recent development, challenges, and prospects*. The AAPS journal, 2021. **23**(4): p. 78.
138. Herrero, M.J., et al., *Physical Methods of Gene Delivery*, in *Safety and Efficacy of Gene-Based Therapeutics for Inherited Disorders*, N. Brunetti-Pierri, Editor. 2017, Springer International Publishing: Cham. p. 113-135.
139. Aliouat, H., et al., *Pure DNA scaffolded drug delivery systems for cancer therapy*. Biomaterials, 2022. **285**: p. 121532.
140. Gill, D.R., I.A. Pringle, and S.C. Hyde, *Progress and Prospects: The design and production of plasmid vectors*. Gene Therapy, 2009. **16**(2): p. 165-171.
141. Seow, Y. and M.J. Wood, *Biological gene delivery vehicles: beyond viral vectors*. Molecular therapy, 2009. **17**(5): p. 767-777.
142. Thakore, P.I. and C.A. Gersbach, *Chapter 3 - Genome Engineering for Therapeutic Applications*, in *Translating Gene Therapy to the Clinic*, J. Laurence and M. Franklin, Editors. 2015, Academic Press: Boston. p. 27-43.
143. Barreto, S.C., M. Uppalapati, and A. Ray, *Small Circular DNAs in Human Pathology*. Malays J Med Sci, 2014. **21**(3): p. 4-18.
144. Tolmachov, O., *Designing plasmid vectors*. Gene Therapy of Cancer: Methods and Protocols, 2009: p. 117-129.
145. Abdulrahman, A. and A. Ghanem, *Recent advances in chromatographic purification of plasmid DNA for gene therapy and DNA vaccines: A review*. Analytica Chimica Acta, 2018. **1025**: p. 41-57.
146. Ghanem, A., R. Healey, and F.G. Adly, *Current trends in separation of plasmid DNA vaccines: a review*. Anal Chim Acta, 2013. **760**: p. 1-15.
147. Duprey, A. and E.A. Groisman, *The regulation of DNA supercoiling across evolution*. Protein Science, 2021. **30**(10): p. 2042-2056.
148. Martinez, M.G., et al., *Covalently closed circular DNA: the ultimate therapeutic target for curing HBV infections*. Journal of hepatology, 2021. **75**(3): p. 706-717.
149. Kadam, N.R. and P.M. Kasar, *DNA*. Asian Journal of Research in Pharmaceutical Science, 2023. **13**(3).
150. Adepu, S. and S. Ramakrishna, *Controlled Drug Delivery Systems: Current Status and Future Directions*. Molecules, 2021. **26**(19): p. 5905.
151. Costa, D., W.H. Briscoe, and J. Queiroz, *Polyethylenimine coated plasmid DNA–surfactant complexes as potential gene delivery systems*. Colloids and Surfaces B: Biointerfaces, 2015. **133**: p. 156-163.
152. Gavas, S., S. Quazi, and T.M. Karpiński, *Nanoparticles for cancer therapy: current progress and challenges*. Nanoscale research letters, 2021. **16**(1): p. 173.
153. Jahangirian, H., et al., *A review of drug delivery systems based on nanotechnology and green chemistry: green nanomedicine*. Int J Nanomedicine, 2017. **12**: p. 2957-2978.
154. Debnath, S.K. and R. Srivastava, *Drug delivery with carbon-based nanomaterials as versatile nanocarriers: progress and prospects*. Frontiers in Nanotechnology, 2021. **3**: p. 644564.
155. Chen, S., et al., *Inorganic Nanomaterials as Carriers for Drug Delivery*. Journal of Biomedical Nanotechnology, 2016. **12**(1): p. 1-27.
156. Mitragotri, S. and P. Stayton, *Organic nanoparticles for drug delivery and imaging*. Mrs Bulletin, 2014. **39**(3): p. 219-223.

157. Bozzuto, G. and A. Molinari, *Liposomes as nanomedical devices*. International journal of nanomedicine, 2015: p. 975-999.
158. Mittal, P., et al., *Dendrimers: A New Race of Pharmaceutical Nanocarriers*. BioMed Research International, 2021. **2021**(1): p. 8844030.
159. Sarkar, C., et al., *PLGA Nanoparticles in Drug Delivery*, in *Nanoengineering of Biomaterials*. 2022. p. 217-260.
160. Wilson, R.J., et al., *Nanoemulsions for drug delivery*. Particuology, 2022. **64**: p. 85-97.
161. Siddique, S. and J.C.L. Chow, *Gold Nanoparticles for Drug Delivery and Cancer Therapy*. Applied Sciences, 2020. **10**(11): p. 3824.
162. Soumya, K., et al., *A comprehensive review on carbon quantum dots as an effective photosensitizer and drug delivery system for cancer treatment*. Biomedical Technology, 2023. **4**: p. 11-20.
163. Kankala, R.K., et al., *Nanoarchitectured structure and surface biofunctionality of mesoporous silica nanoparticles*. Advanced materials, 2020. **32**(23): p. 1907035.
164. Vallet-Regí, M., *Our contributions to applications of mesoporous silica nanoparticles*. Acta Biomaterialia, 2022. **137**: p. 44-52.
165. Allen, M.J., V.C. Tung, and R.B. Kaner, *Honeycomb carbon: a review of graphene*. Chemical reviews, 2010. **110**(1): p. 132-145.
166. Daniyal, M., B. Liu, and W. Wang, *Comprehensive review on graphene oxide for use in drug delivery system*. Current Medicinal Chemistry, 2020. **27**(22): p. 3665-3685.
167. Jha, R., et al., *Smart carbon nanotubes for drug delivery system: A comprehensive study*. Journal of Drug Delivery Science and Technology, 2020. **58**: p. 101811.
168. Kiran, A.R., G.K. Kumari, and P.T. Krishnamurthy, *Carbon nanotubes in drug delivery: Focus on anticancer therapies*. Journal of Drug Delivery Science and Technology, 2020. **59**: p. 101892.
169. Derakhshankhah, H. and S. Jafari, *Cell penetrating peptides: A concise review with emphasis on biomedical applications*. Biomedicine & Pharmacotherapy, 2018. **108**: p. 1090-1096.
170. Gessner, I. and I. Neundorf, *Nanoparticles modified with cell-penetrating peptides: Conjugation mechanisms, physicochemical properties, and application in cancer diagnosis and therapy*. International journal of molecular sciences, 2020. **21**(7): p. 2536.
171. Desale, K., K. Kuche, and S. Jain, *Cell-penetrating peptides (CPPs): An overview of applications for improving the potential of nanotherapeutics*. Biomaterials Science, 2021. **9**(4): p. 1153-1188.
172. Neves, A.R., et al., *Development of WRAP5 Peptide Complexes for Targeted Drug/Gene Co-Delivery toward Glioblastoma Therapy*. Pharmaceutics, 2022. **14**(10): p. 2213.
173. Hassanin, I. and A. Elzoghby, *Albumin-based nanoparticles: a promising strategy to overcome cancer drug resistance*. Cancer Drug Resist, 2020. **3**(4): p. 930-946.
174. Solanki, R., et al., *Anticancer nano-delivery systems based on bovine serum albumin nanoparticles: A critical review*. International Journal of Biological Macromolecules, 2021. **193**: p. 528-540.
175. Gregory, J.V., et al., *Systemic brain tumor delivery of synthetic protein nanoparticles for glioblastoma therapy*. Nature Communications, 2020. **11**(1): p. 5687.
176. Li, X., et al., *Albumin-binding photosensitizer capable of targeting glioma via the SPARC pathway*. Biomaterials Research, 2023. **27**(1): p. 23.
177. Parveen, M., et al., *Isolation, Characterization, and Single-Crystal X-ray Analysis of Lantabetulic Acid from Rhus alata: Insights into HSA and BSA*

Binding Interactions, with In-Silico Study. ACS Omega, 2024. **9**(38): p. 39484-39502.
178. Mishra, V. and R.J. Heath, *Structural and Biochemical Features of Human Serum Albumin Essential for Eukaryotic Cell Culture*. Int J Mol Sci, 2021. **22**(16).
179. Ikeda-Imafuku, M., et al., *Strategies to improve the EPR effect: A mechanistic perspective and clinical translation*. Journal of Controlled Release, 2022. **345**: p. 512-536.
180. Li, X., et al., *Albumin-binding photosensitizer capable of targeting glioma via the SPARC pathway*. Biomaterials Research, 2023. **27**(1): p. 23.
181. N. Politis, S., et al., *Design of experiments (DoE) in pharmaceutical development*. Drug development and industrial pharmacy, 2017. **43**(6): p. 889-901.
182. Tavares Luiz, M., et al., *Design of experiments (DoE) to develop and to optimize nanoparticles as drug delivery systems*. European Journal of Pharmaceutics and Biopharmaceutics, 2021. **165**: p. 127-148.
183. Adena, S.K.R., et al., *Development, optimization, and in vitro characterization of dasatinib-loaded PEG functionalized chitosan capped gold nanoparticles using Box–Behnken experimental design*. Drug development and industrial pharmacy, 2018. **44**(3): p. 493-501.
184. Alam, T., et al., *Adaptation of Quality by Design-Based Development of Isradipine Nanostructured–Lipid Carrier and Its Evaluation for In Vitro Gut Permeation and In Vivo Solubilization Fate*. Journal of Pharmaceutical Sciences, 2018. **107**(11): p. 2914-2926.
185. Bachhav, S.S., et al., *Rifampicin Lipid-Polymer hybrid nanoparticles (LIPOMER) for enhanced Peyer's patch uptake*. International Journal of Pharmaceutics, 2017. **532**(1): p. 612-622.
186. Chauhan, M.K. and N. Bhatt, *Bioavailability enhancement of polymyxin B with novel drug delivery: development and optimization using quality-by-design approach*. Journal of Pharmaceutical Sciences, 2019. **108**(4): p. 1521-1528.
187. Dawoud, M.H.S., et al., *Insulin Mucoadhesive Liposomal Gel for Wound Healing: a Formulation with Sustained Release and Extended Stability Using Quality by Design Approach*. AAPS PharmSciTech, 2019. **20**(4): p. 158.
188. Hosny, K.M., K.M. El-Say, and H.M. Alkhalidi, *Quality by design approach to screen the formulation and process variables influencing the characteristics of carvedilol solid lipid nanoparticles*. Journal of Drug Delivery Science and Technology, 2018. **45**: p. 168-176.
189. Rodolfo, C., et al., *Design of Experiments to Achieve an Efficient Chitosan-Based DNA Vaccine Delivery System*. Pharmaceutics, 2021. **13**(9): p. 1369.
190. Jankovic, A., G. Chaudhary, and F. Goia, *Designing the design of experiments (DOE) – An investigation on the influence of different factorial designs on the characterization of complex systems*. Energy and Buildings, 2021. **250**: p. 111298.
191. Oyejola, B. and J. Nwanya, *Selecting the right central composite design*. International Journal of Statistics and Applications, 2015. **5**(1): p. 21-30.
192. Neves, A.R., et al., *Development of WRAP5 Peptide Complexes for Targeted Drug/Gene Co-Delivery toward Glioblastoma Therapy*. Pharmaceutics, 2022. **14**(10).
193. Karimi, M., et al., *Albumin nanostructures as advanced drug delivery systems*. Expert Opinion on Drug Delivery, 2016. **13**(11): p. 1609-1623.
194. Babcock, J.J. and L. Brancaleon, *Bovine serum albumin oligomers in the E- and B-forms at low protein concentration and ionic strength*. Int J Biol Macromol, 2013. **53**: p. 42-53.
195. Merlot, A.M., D.S. Kalinowski, and D.R. Richardson, *Unraveling the mysteries of serum albumin-more than just a serum protein*. Front Physiol, 2014. **5**: p. 299.

196. Li, X., et al., *Albumin-binding photosensitizer capable of targeting glioma via the SPARC pathway*. Biomater Res, 2023. **27**(1): p. 23.
197. Nosrati, H., et al., *Bovine Serum Albumin (BSA) coated iron oxide magnetic nanoparticles as biocompatible carriers for curcumin-anticancer drug*. Bioorganic Chemistry, 2018. **76**: p. 501-509.
198. Al-Jawad, S.M.H., et al., *Synthesis and characterization of small-sized gold nanoparticles coated by bovine serum albumin (BSA) for cancer photothermal therapy*. Photodiagnosis and Photodynamic Therapy, 2018. **21**: p. 201-210.
199. Fan, D., et al., *Nanomedicine in cancer therapy*. Signal Transduction and Targeted Therapy, 2023. **8**(1): p. 293.
200. Jin, C., et al., *Application of Nanotechnology in Cancer Diagnosis and Therapy - A Mini-Review*. Int J Med Sci, 2020. **17**(18): p. 2964-2973.
201. Kemp, J.A. and Y.J. Kwon, *Cancer nanotechnology: current status and perspectives*. Nano Convergence, 2021. **8**(1): p. 34.
202. Ben Ali, R., et al., *Bisphenol A removal by the Chlorophyta Picocystis sp.: optimization and kinetic study*. Int J Phytoremediation, 2021. **23**(8): p. 818-828.
203. Sankha, B., *Central Composite Design for Response Surface Methodology and Its Application in Pharmacy*, in *Response Surface Methodology in Engineering Science*, K. Palanikumar, Editor. 2021, IntechOpen: Rijeka. p. Ch. 5.
204. Patil, S.A., et al., *Optimization of medium using response surface methodology for l-DOPA production by Pseudomonas sp. SSA*. Biochemical Engineering Journal, 2013. **74**: p. 36-45.
205. Amighi, F., Z. Emam-Djomeh, and M. Labbafi-Mazraeh-Shahi, *Effect of different cross-linking agents on the preparation of bovine serum albumin nanoparticles*. Journal of the Iranian Chemical Society, 2020. **17**(5): p. 1223-1235.
206. Pirkhezranian, Z., et al., *Interaction of camel Lactoferrin derived peptides with DNA: a molecular dynamics study*. BMC Genomics, 2020. **21**(1): p. 60.
207. Davis, H.C., N.D. Posey, and G.N. Tew, *Protein Binding and Release by Polymeric Cell-Penetrating Peptide Mimics*. Biomacromolecules, 2022. **23**(1): p. 57-66.
208. Aramesh-Boroujeni, Z., et al., *Evaluation of parent and nano-encapsulated terbium(III) complex toward its photoluminescence properties, FS-DNA, BSA binding affinity, and biological applications*. Journal of Trace Elements in Medicine and Biology, 2020. **61**: p. 126564.
209. Galdino, F.E., et al., *Effect of particle functionalization and solution properties on the adsorption of bovine serum albumin and lysozyme onto silica nanoparticles*. Colloids and Surfaces B: Biointerfaces, 2020. **186**: p. 110677.
210. Srivastava, A. and A. Prajapati, *Albumin and functionalized albumin nanoparticles: production strategies, characterization, and target indications*. Asian Biomedicine, 2020. **14**(6): p. 217-242.
211. Luis de Redín, I., et al., *Human serum albumin nanoparticles for ocular delivery of bevacizumab*. International Journal of Pharmaceutics, 2018. **541**(1): p. 214-223.
212. Bukackova, M. and R. Marsalek, *Interaction of BSA with ZnO, TiO2, and CeO2 nanoparticles*. Biophysical Chemistry, 2020. **267**: p. 106475.
213. Li, Z., D. Lu, and X. Gao, *Optimization of mixture proportions by statistical experimental design using response surface method - A review*. Journal of Building Engineering, 2021. **36**: p. 102101.
214. Lakka, N.S., et al., *Degradation pathways and impurity profiling of the anticancer drug apalutamide by HPLC and LC–MS/MS and separation of impurities using Design of Experiments*. Biomedical Chromatography, 2023. **37**(2): p. e5549.
215. Rasmussen, M.K., J.N. Pedersen, and R. Marie, *Size and surface charge characterization of nanoparticles with a salt gradient*. Nature Communications, 2020. **11**(1): p. 2337.

216. Foroozandeh, P. and A.A. Aziz, *Insight into Cellular Uptake and Intracellular Trafficking of Nanoparticles*. Nanoscale Research Letters, 2018. **13**(1): p. 339.
217. Filippov, S.K., et al., *Dynamic light scattering and transmission electron microscopy in drug delivery: a roadmap for correct characterization of nanoparticles and interpretation of results*. Materials Horizons, 2023. **10**(12): p. 5354-5370.
218. Farkas, N. and J.A. Kramar, *Dynamic light scattering distributions by any means*. Journal of Nanoparticle Research, 2021. **23**(5): p. 120.
219. Baranov, M.V., et al., *Modulation of immune responses by particle size and shape*. Frontiers in immunology, 2021. **11**: p. 607945.
220. Valente, J.F.A., et al., *Purification of supercoiled p53-encoding plasmid using an arginine-modified macroporous support*. J Chromatogr A, 2020. **1618**: p. 460890.
221. Lee, Y.-J., et al., *Gene expression profiling of glioblastoma cell lines depending on TP53 status after tumor-treating fields (TTFields) treatment*. Scientific Reports, 2020. **10**(1): p. 12272.
222. *ISO 10993-5: 2009. Biological Evaluation of Medical Devices. Part 5: Tests for In Vitro Cytotoxicity*, I.O.f. Standardization, Editor. 2009: Geneva, Switzerland.
223. Liang, J., et al., *Menthol-modified BSA nanoparticles for glioma targeting therapy using an energy restriction strategy*. NPG Asia Materials, 2019. **11**(1): p. 38.
224. Liu, Y., et al., *Fluorescent bovine serum albumin-silver nanoclusters loaded with paclitaxel can traverse the blood-brain barrier to inhibit the migration of glioma*. Journal of Bio-X Research, 2020. **03**(04): p. 183-192.

Chapter 7- Annexes

Figure 23. Presence certificate to Annual CICS-UBI Symposium.

Figure 24. Scientific publication "Design of Experiments to Tailor the Potential of BSA-Coated Peptide Nanocomplexes for Temozolomide/p53 Gene Co-Delivery" (https://www.mdpi.com/1999-4923/16/11/1389)